METEOR-Bericht

Sector collapse kinematics and tsunami implications – SEKT

Cruise No. M154/1

April 3 – April 25, 2019

Mindelo (Cape Verde) – Point-á-Pitre (Guadeloupe)

With contributions by Christoph Böttner, Judith Elger, Stefan Kontradowitz, Michel Kühn, Sebastian Müller, Bettina Schramm and Martin Stelzner

C. Berndt

GEOMAR Helmholtz Centre for Ocean Research Kiel

2019

Table of Content

1 Cruise Summary

1.1 Summary in English

Deep-seated collapses of volcanic islands have generated the largest volume mass flows worldwide. These mass flows might trigger mega-tsunamis. The way in which these collapse events are emplaced is poorly understood, even though this emplacement process determines the scale of associated tsunamis.

Key questions such as whether they are emplaced in single or multiple events, how they may incorporate seafloor sediment to increase their volume, and how they are related to volcanic eruption cycles and migration of volcanic centers, remain to be answered.

This project forms a part of the comprehensive study of large volcanic island landslide deposits and is directly linked to IODP drilling campaign in the Lesser Antilles (IODP Leg 340). Unfortunately, Leg 340 only recovered material from a single site within the volcanic landslide deposits off Montserrat, and even at this site, recovery was not continuous. This single IODP site is insufficient to document lateral variation in landslide character, which is critical for understanding how it was emplaced. The main scientific goals of this project are to determine where the landslides are sourced from; to understand how these landslides are emplaced; and to understand the relationship between landslides, eruption cycles and initiation of new volcanic centres. Combining 3D seismology (Leg 1) and MeBo cores (Leg 2) provides a unique dataset of the internal structure, composition and source of material throughout a volcanic island landslide. The results will significantly contribute to understanding the emplacement of volcanic island landslides and they will allow us to assess the associated tsunami risk.

1.2 Zusammenfassung

Hangrutschungen, die bei Flankenkollapsen vulkanischer Ozeaninseln entstehen, zählen zu den größten Rutschungen weltweit und können möglicherweise Mega-Tsunamis auslösen. Da die Dynamik der Kollapsereignisse ein entscheidender Faktor ist, jedoch schwer zu bestimmen, wird die Höhe der Tsunamis kontrovers diskutiert. Hauptfragestellungen sind dabei, ob die initialisierte Unterwasserrutschung in einem einzelnen oder in mehreren Ereignissen stattfindet, inwieweit neben dem initial destabilisierten Material weitere Sedimente mittransportiert werden, und wie sie mit Vulkanausbruchszyklen und der Migration von vulkanischen Zentren zusammenhängen.

M154 baut auf der ersten groß angelegten interdisziplinären Untersuchung der Rutschungsablagerungen von Vulkaninseln und einer IODP-Bohrung bei den Kleinen Antillen (IODP Leg 340). Leider wurde nur ein unvollständiger Kern innerhalb der vulkanischen Hangrutschungen vor Montserrat erbohrt. Informationen über laterale Änderung der Hangrutschung können auf der bisherigen Datenbasis nicht erforscht werden, obwohl diese für das Verständnis des Ablagerungsprozesses von entscheidender Bedeutung sind. Die Kombination von Bohrungen und 3D Seismik hat einen einmaligen Datensatz zur Untersuchung der internen Strukturen, der Zusammensetzung und der Herkunft des Materials der vulkanischen Rutschmassen ergeben. Die Ergebnisse sollen zum Verständnis der Prozesse beitragen, die während vulkanischer Hangrutschungen aktiv sind und so eine Quantifizierung des Tsunamipotentials erlauben. Die wichtigsten wissenschaftlichen Ziele der Ausfahrt sind es, zu bestimmen, woher die Rutschmassen stammen; wie diese abgelagert werden; und den

Zusammenhang zwischen Hangrutschungen, Ausbruchszyklen und der Initiierung neuer Vulkanzentren zu verstehen.

2 Participants

2.1 Principal Investigators

Name	Institution
Berndt, Christian, Prof.	GEOMAR

2.2 Scientific Party

Name	Discipline	Institution
Prof. Dr. Berndt, Christian	Chief Scientist	GEOMAR
Kühn, Michel	Seismic processing, HiWi	GEOMAR
Dr. Elger, Judith	P-Cable seismic	GEOMAR
Böttner, Christoph	Hydroacoustics	GEOMAR
Schramm, Bettina	OBS	GEOMAR
Wetzel, Gero Klas	Technician: P-Cable	GEOMAR
Ernst, Adrian	Technician, HiWi	GEOMAR
Prof. Dr. Micaleff, Aaron	Scientist	UM
Kontradowitz, Stefan	OBS, Watch keeping, Administration	GEOMAR
Prof. Dr. Chi, Wu-Cheng	Scientist	Sinica
Kunath, Pascal	Watch keeping, PhD	NTU
Finger, Nils-Peter	Watch keeping, PhD	GFZ
Kaminski,Pauline	Watch keeping, HiWi	TUHH
Hollenberg, Insa	Watch keeping, HiWi	Muthesius
Dr. Müller, Sebastian	Scientist	MPI
Wilckens, Christina Henriette	Watch keeping, HiWi	CAU
Lohrberg, Arne	Watch keeping, PhD	CAU
Kunde, Dennis	Watch keeping, HiWi	CAU
Gamarra Chu, Cony	Watch keeping, HiWi	CAU
Stelzner, Martin	Meteorology	DWD

2.3 Participating Institutions

GEOMAR	Helmholtz-Zentrum für Ozeanforschung Kiel
CAU	Christian-Albrechts-Universität zu Kiel
DWD	Deutscher Wetterdienst, Geschäftsfeld Seeschifffahrt
GFZ	Deutsche GeoForschungsZentrum
MPI	Max-Planck-Institut für Meteorologie
TUHH	Technische Universität Hamburg
Sinica	Academica Sinica
Muthesius	Kunsthochschule Kiel
NTU	National Taiwan University
MU	University of Malta

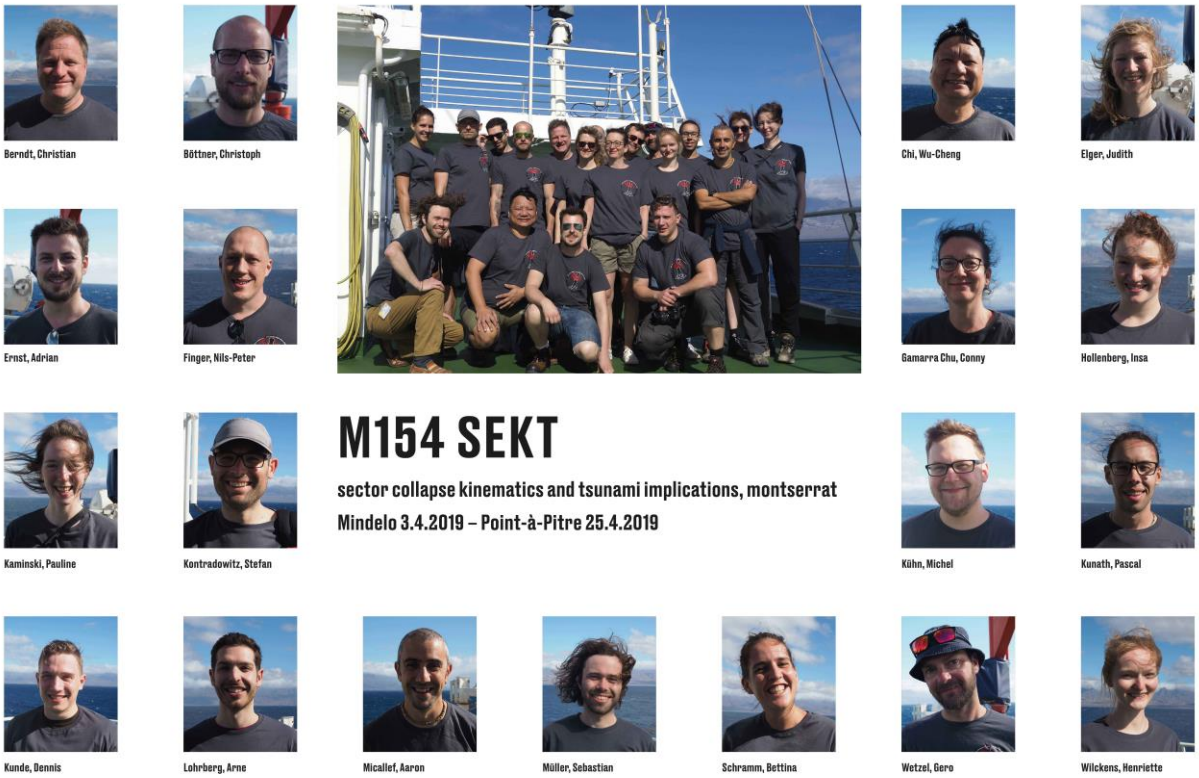

Fig. 2.1: Scientific Party of RV METEOR Cruise M154/1.

2.4 Crew

Name	**Rank**
Hammacher, Rainer	Kapitän / Master
Soßna, Yves Michael	Chiefmate / Chiefmate
Werner, Lena	1. Offizier / First Mate
Mock, Benjamin	2. Offizier / 2nd Officer
Neumann, Peter	Ltd. Ingenieur / Chief Engineer
Brandt, Björn	2. Ingenieur / 2nd Engineer
Heitzer, Ralf	2. Ingenieur / 2nd Engineer
Mehlig, Olaf	SET / Electrical Engineer
Lange, Gerhard	Decksschlosser / Fitter
Schroeder Manfred	Motorenwärter / Motorman
Lukas Eller	Motorenwärter / Motorman
Erdmann, Ole	Motorenwärter / Motorman
Willms, Olaf	Ltd. Elektroniker / Chief Electronic
Hebold, Cathi	Elektroniker / Electronic
Bagyura, Bernhard	Systemmanager / Systemmanager
Wolf, Alexander	Bootsmann / Boatswain
Hildebrandt, Hubert	Matrose / Sailor
Behlke, Hans	Matrose / Sailor

Drakopoulos, Evgenios	Matrose / Sailor
Zeigert, Michael	Matrose / Sailor
de Moliner, Ralf	Matrose / Sailor
Schabeck, Henry	Matrose / Sailor
Lison, Olaf	Matrose / Sailor
Staffeldt, Felix	Azubi / Apprentice
Mönnich, Niklas	Azubi / Apprentice
Hinz, Michael	Arzt / Doctor
Tomaschewski, Joanna	Praktikantin / Trainee
Tober, Martina	1. Steward / Chief Steward
Jürgens, Moni	2. Stewardess / 2. Stewardess
Schmandke, Harald	2. Steward / 2. Steward
Zhang, Gou Min	Wäscher / Laundry Master
Wernitz, Peter	Koch / Cook
Kosanke, Patrick	Kochsmaat / 2nd Cook

3 Research Program

3.1 Description of the Work Area

The island of Montserrat in the Lesser Antilles is an ideal natural laboratory to study volcanic island landslide processes. Previous seismic data document the location of more than ten large landslide deposits around the island (Le Friant et al., 2004; LeBas et al., 2011; Watt et al., 2012a; Crutchley et al., 2013; Karstens et al., 2013). In several locations of Montserrat blocky flank collapse deposits and more extensive, smoother deposits occur together (Watt et al., 2012b). With high-resolution geophysical data we were able show that this emplacement relationship involves events dominated by seafloor sediment failure. The volume of the landslide deposits cannot be explained by the failure of volcanic material alone. Additionally, internal structures show that deposit emplacement may occur in multiple stages. Sediment failure is associated with elongate deposits but with relatively little downslope material motion. Although of greater volume, the sediment failure component of these landslides produces small tsunamis in comparison to the volcanic component, which presents a more significant local hazard. This would suggest that some of the claims concerning tsunami height that were made for other volcanic islands (e.g. Canary Islands) were grossly exaggerated.

Two of the Montserrat landslides with contrasting character (Deposits 1 and 2) will be focus of this project. These landslides are relatively small, and we are therefore able to map them completely in a reasonable time frame. Deposit 1 (1.7 km3) is the most recent event, has a blocky character, and is draped by only ~1-2 meters of sediment. Deposit 2 is much more extensive, has a smoother surface, and appears to contain a significant component of incorporated sea floor sediment. The more deeply buried Deposit 2 is overlain by 5 to 10 m of drape. Deposit 2 is up to 90 m thick, and comprises two parts (Deposits 2a and 2b) separated by laterally extensive seismic reflectors. Emplacement of Deposit 2 appears to have triggered large-scale failure of sea floor sediment, as documented by a major head scarp along the northeastern limit of the deposit (Fig. 3.1).

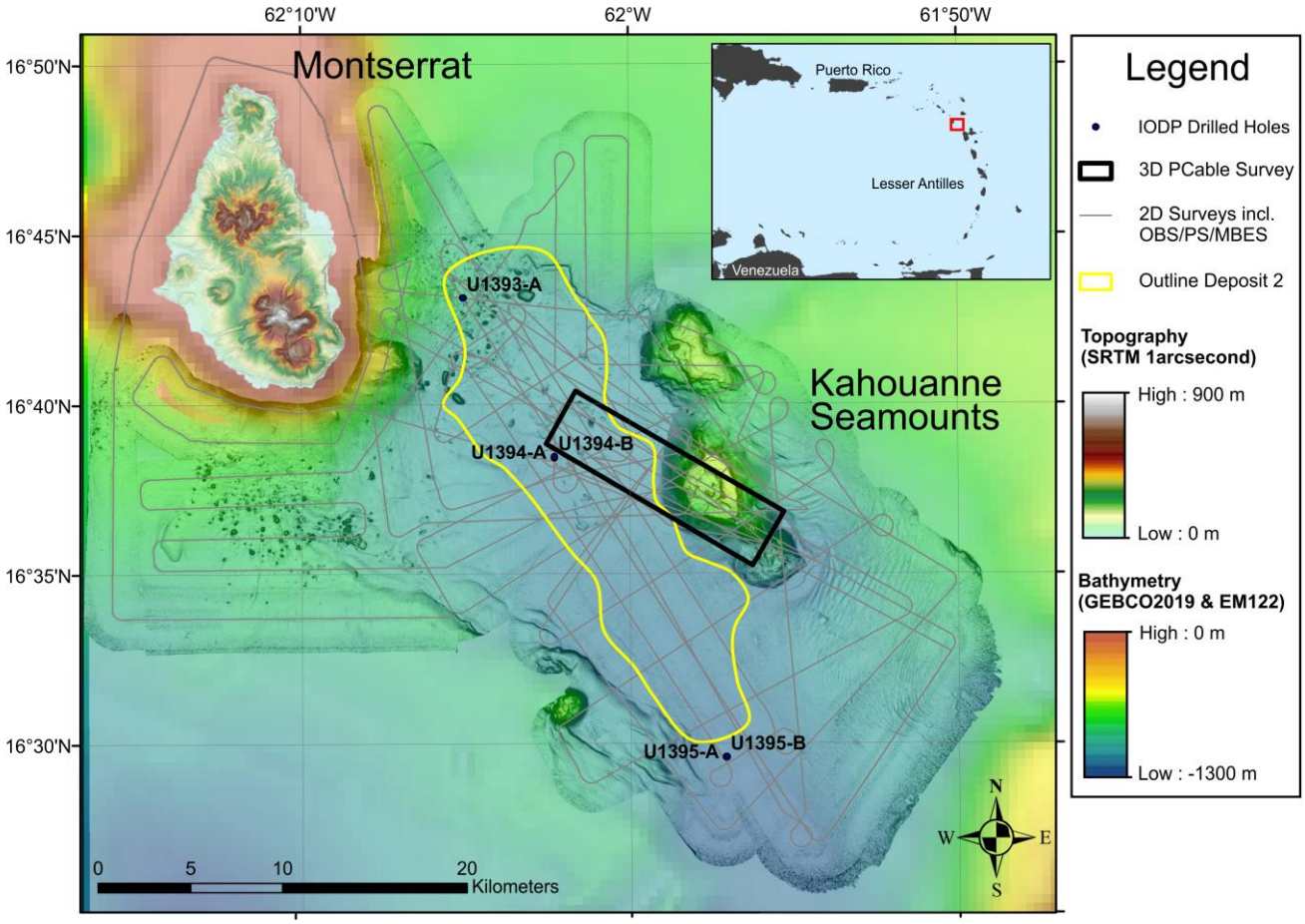

Fig. 3.1: Working area of RV METEOR Cruise M154/1.

3.2 Aims of the Cruise

The collapse of volcanic islands can generate extremely large landslides. This is why this type of landslide is so dangerous, both due to the initial slide itself and through far field tsunami generation. Volcanic island landslides can have volumes of up to several thousand cubic kilometers. For instance, the Nuuanu landslide off Oahu (Hawaiian Islands) has a volume of ~5,000 km3 (Moore et al., 1989), making it the largest volume mass flows yet mapped on our planet. The largest known landslide found on land occurs on Mt Shasta and has a volume of only ~45 km3 (Crandell, 1989). For comparison, the flank collapse that occurred during the well-known 1980 eruption of Mt St Helens had a volume of ~ 3 km3 (Sousa and Voight, 1995).

Sea floor mapping has shown that major landslide deposits are common around volcanic islands worldwide. The first systematic study was carried out along the Hawaiian Ridge, revealing at least 68 major landslides along a 2,200-km stretch of the ridge (McMurtry et al., 2004; Moore et al., 1995; Moore et al., 1989; Moore and Normark, 1994; Williams et al., 2006). Since then major debris avalanches have been identified around numerous oceanic island groups including the Marquesas Islands (Wolfe et al., 1994), La Réunion (Labazuy, 1996), the Cape Verde Islands (Masson et al., 2008), the Lesser Antilles (Deplus et al., 2001; Boudon et al., 2007), and the Canary Islands (Krastel et al., 2001; Masson et al., 2002; Urgeles et al., 1999; Watts and Masson, 1995). Giant submarine landslides play an important role during the evolution of volcanic islands, especially during the shield phase of volcanic islands, when high

amounts of extrusive and intrusive magmatic activity leads to the quick build-up of potentially unstable volcanic edifices (Krastel et al., 2001; Moore et al., 1989).

There is considerable controversy over the likely magnitudes of tsunamis generated by volcanic island landslides, and hence the hazard they may pose. We need to better understand how submarine landslides are emplaced because it is this emplacement process that determines the tsunami magnitude. In particular, we need to understand (1) where the material originates in the landslide, and (2) whether the landslide was emplaced in one or multiple stages.

Origin of material in the landslide: The original source of material within the landslide has a strong control on the scale of tsunami produced by a landslide (Watt et al., 2012a). The volume is the one of the most critical parameter for tsunami generation. For the same unit volume, however, a landslide originating on the submerged flanks of the volcano, and especially from the sea floor, will produce a smaller tsunami than a landslide comprising only the subaerial volcanic edifice. As noted by Watt et al. (2012a), a landslide offshore Montserrat would have produced significantly smaller tsunamis if much of the material within them is sea floor sediment rather than parts of the volcanic edifice. (Watt et al., 2012a). A central objective of this project is a detailed analysis of a landslide deposits off Montserrat by MeBo drilling and 3D-seismic imaging in order to investigate the origin of the material in different parts of the landslide.

Emplacement process: Tsunami magnitude is also critically dependent on whether failure occurs in one stage or in many separate stages. Failure in a series of stages separated by a few tens of seconds or minutes can substantially reduce the resulting tsunami magnitude (Løvholt et al., 2005,). Landslide deposits can be relatively complex, and it is often the turbidity current that runs out beyond the landslide that provides the clearest record of emplacement dynamics. For instance, Hunt et al. (2011) showed how the turbidite associated with the Icod volcanic landslide in the Canary Island comprises a series of compositionally distinct sub-units, which record multistage collapse. The presence of turbidite mud intervals within these subunits, which would take a considerable period to settle, suggests considerable delays between each sub-stage of the collapse. IODP site U1395 offshore Montserrat recovered the distal turbidite associated with volcanic landslide Deposit 2 (see Fig. 3.1 for location). It comprises a series of massive fining-up sand intervals forming a spectacular 7 m thick deposit some 25 km from the volcano. Further MeBo cores from the distal run-out turbidite deposit shall be drilled in the frame of this proposal in order ensure that this was a single stage event. Submarine landslides from offshore from a volcanic island can be extremely large, and may pose a significant hazard, both from the landslide itself, and from resulting tsunamis. The emplacement dynamics of these landslides and their relationship to volcanic eruption cycles or magmatic evolution are poorly understood at present, due to a lack of detailed studies of landslide deposits.

Based on the circumstances described above the first aim of this project is to determine where the landslides are sourced from, the volcanic edifice or from the sedimentary slope around ocean islands; the second aim is to understand how they are emplaced. The third aim is to understand the relationship between landslides, eruption cycles and initiation of new volcanic centres.

3.2.1 What type of material are the landslides made of, and where did that material originate? How much sea floor sediment was incorporated into the landslides, and by what processes? What are the implications for tsunami generation?

Through combination of the MeBo cores collected during leg 2 and 2D and 3D seismic data we will document the spatial variability and overall character of Deposit 2. This work will constrain the relative fraction of material from the volcanic edifice and seafloor sediment within the landslide. The single IODP site (U1394) that penetrated Deposit 2 shows that it is overlain by a very heterogeneous mass flow deposit that contains a range of volcanic and bioclastic material. However, it leaves two possible hypotheses for the origin of flat lying interbedded sand and mud intervals that form the lower part of Deposit 2, which are separated by homogenised sediments resembling debris flow matrix. The first hypothesis is that the packages of flat lying sediment are blocks of sediment incorporated into the landslide. The second hypothesis is that the flat lying sediment and debritic intervals are undeformed and in-situ and record a very prolonged multistage collapse of the volcano. This project aims to test the validity of these contrasting hypotheses.

A major scarp on the sea floor is inferred to record failure of sea floor sediment associated with Deposit 2. We have investigated the frontal and lateral margins of Deposits 2 and 8 using the new unusually detailed 3D seismic data. It is enigmatic that the front of landslide Deposit 8 seems not to emerge above the pre-existing seabed. Instead of being emplaced onto the pre-existing seafloor they seem to bulldoze into the sediments and produce a long but abruptly terminated snout of shortened pre-existing seafloor material. The lateral margin of Deposit 2 can also comprises a sharp transition from chaotic reflectors to laterally equivalent undeformed strata, which suggests that well bedded sea floor sediment has been incorporated into the landslide. If this is the case, then the incorporated sea floor sediment may be deformed but not far travelled. Similar structures appear to exist in the limited available 2D seismic profiles from debris avalanches offshore Dominica, Martinique and St Lucia. Thus, this raises the question of whether margins of this type are common around submarine landslides offshore volcanic islands, even though they are relatively unusual in other settings (Frey Martinez et al. 2006). By obtaining data from these several sites, we may thus be able to offer new and important insights into general processes of mass movement in seafloor sediment that may occur during the submarine emplacement of volcanic debris avalanches.

3.2.2 Have the landslides been emplaced in one or multiple events?

Understanding whether volcanic island landslides are emplaced in a single short-lived episode, or in multiple stages, is crucially important for predicting the magnitude of resulting tsunamis. Emplacement in multiple stages (even a few minutes apart) can greatly reduce initial tsunami magnitude (e.g. by > 50% Løvholt et al., 2005). The MeBo cores in combination with 3D seismic data will constrain the significance of internal reflectors within Deposit 2, and whether these reflectors record emplacement in one or multiple stages.

The deposits of longer run out turbidity currents can also be used to determine whether the associated landslide was emplaced in one or multiple stages (Wynn and Masson, 2003; Hunt et al., 2011). Turbidites that comprise multiple fining up sequences of sand capped by mud indicate

emplacement in multiple widely spaced stages, as mud settles and consolidates slowly. At IODP site U1395, the spectacular 7 m thick turbidite associated with Deposit 2 comprise a series of stacked graded sand units without intervening mud. This suggests that Deposit 2 was emplaced in a series of closely spaced pulses. However, an alternative explanation is that the mud drapes were removed by later stages of the flow.

3.2.3 What is the timing of major landslides relative to volcanic eruption cycles, initiation of new volcanic centres, or sea level change?

It is important to understand the timing of major landslide events relative to eruption cycles for hazard predictions. An exciting initial observation from IODP Leg 340 is that Deposit 2 is immediately overlain by a basaltic fallout deposit, suggesting it may be associated with a major change in magma composition, and initiation of the basaltic South Soufriere Hills centre on Montserrat. IODP core U1396 provides an excellent record of over 140 fallout layers during the last 4.5 Ma. However, during some periods the direction of the wind would not be towards this site, and the fallout from eruptions would be elsewhere. Analysis of fallout deposits within the widely spaced MeBo and gravity cores will help to provide a more complete record of major volcanic eruptions on Montserrat. These core data will also help to determine precisely the emplacement age of Deposits 1 and 2.

The most crucial task during the cruise was the collection of a high-resolution 3D seismic cube – using the P-Cable seismic system –extending the cube collected in 2010 out beyond the edge of debris avalanche deposit. With this cube, it is possible a) to determine whether the crucial Deposit 2 consists of two events or if it was caused by one event that changes character laterally, b) to determine the amount of erosion at the slide plane; and c) to determine the geometry at the toe of the deposit. This will be achieved by creating horizon attributes (steering, dip, amplitude, RMS amplitude) and volume attributes (co-herency, similarity, etc.) of the 3D seismic data and integrating them via core-log seismic integration with the results of the two IODP cores within the planned cube and with the information from MeBo drilling during the second leg of the cruise. In order to provide velocity information for the 3D processing after the cruise, we acquired four ocean bottom seismometer (OBS) data sets distributed within the area of the P-Cable cube. The ocean bottom seismometers were deployed before the 3D data acquisition commenced, and were recovered after shooting had stopped.

3.3 Agenda of the Cruise

After sailing across the Atlantic from the Cape Verde Islands, we run a sound velocity probe to calibrated the ship's echosounders and deployed ten ocean bottom seismometers. Upon arrival in the study area off Montserrat, this was followed by the main task of the first leg, i.e. the collection of a high-resolution 3D seismic cube extending the 3D seismic cube collected during JC45 in 2010 out beyond the edge of debris avalanche deposit 2. The collection of the 3D seismic data took 13 working days. Afterwards, we recovered the ocean bottom seismometers. The seismic processing commenced as soon as the first data were collected. Throughout the entire first leg we used the EM712 multibeam echosounder to produce a new bathymetric map of the study area.

4 Narrative of the Cruise

Wednesday, 3.4.2019

We departed from Mindelo at 09:00 local time on April 3 and set sail for Montserrat in the Caribbean. When outside the Cape Verde EEZ we collected a sound velocity profile and used it to calibrate of the hydroacoustic equipment. Then we switched on the deep sea echosounder EM122 and the subbottom profiler Parasound and kept them running until we reached the French EEZ on April 9. The transit across the Atlantic was used to prepare the seismic equipment for the main experiment.

Wednesday, 10.4.2019

We reached the study area off Montserrat at 10:30 am. First we carried out the releaser test for the ocean bottom seismometers and collected another sound velocity profile. From 14:00 onwards we deployed 10 ocean bottom seismometers. This was completed at 20:00. Afterwards we deployed the 2D seismic streamer to shoot profiles along the OBS tracks with a long shot interval of 10 s. The system was up and running at 22:30.

Thursday, 11.4.2019

During the morning, we continued acquiring 2D seismic data along the track lines. After lunch we started to deploy the 3D seismic system which was finished at 17:00 and the first sail line of the 3D seismic cube across Kahouane Seamounts and the central part of deposit 2 started at 18:00. We used sixteen streamers and a shot interval of 5 seconds. Unfortunately, the wind picked up to Bft 5-6 which is not ideal for the quality of the seismic data. At 21:00 the junction box between the cross cable and the data cable had a water intrusion which made it necessary to recover that part of the P-Cable and re-terminate.

Friday, 12.4.2019

Repairs and redeployment took until 2:30 am. Afterwards P-Cable shooting continued. At 14:00 the starboard paravane caught a fishing net and we had to recover the data cable and the first three streamers to fix the system. This took until 17:00 and the P-Cable was redeployed and acquisition continued.

Saturday, 13.4.2019

By midnight, the wind had picked up that the waves caused damage to the data cable and the system had to be recovered. Throughout the night, we re-rigged the system to 2D mode and started acquisition of 2D seismic data with 7 streamers at 7am in the morning. Shooting continued throughout the day.

Sunday, 14.4.2019

At 10 am, the first GI gun started to leak air and the seismic source had to be recovered. We replaced the first gun and resumed shooting at noon.

Monday 15.4.2019

We continued shooting 2D seismic data until noon when the weather calmed down. During the afternoon, we re-rigged the seismic system to P-Cable mode and started data collection at 20:45 in force 5-6 winds.

Tuesday, 16.4.2019

We continued shooting 3D seismic data only interrupted in the morning by a 1.5 h airgun service.

Wednesday, 17.4.2019

At 05:30 the system had to be recovered because the data link broke down. The tension release on the data cable had slipped and the resulting movement had loosened a connector in the junction box. After repairs until 09:30 the system was redeployed and we continued shooting until 12:00 when the second streamer had problems. We had to replace it which took until 14:30 and continued shooting until 16:15 when the system had communication problems again. We reduced the speed to 3 kts through the water to relieve tension on the cross-cable which improved the communication. At 19:00 the portside paravane caught a fishing line. We continued the survey until 23:00 hoping that it would come loose, but it did not and at 23:00 the system broke down and had to be recovered.

Thursday, 18.4.2019

It took until 03:00 to get rid of the fishing line and we deployed a 2D system with two streamer sections to be able to repair the P-Cable using the winch. During the day, we continued 2D data acquisition and replaced all cross-cable segments. At 18:00, we recovered the 2D system and deployed the P-Cable. This took until 22:00 when we resumed shooting 3D data.

Friday, 19.4.2019

We continued 3D data acquisition in winds up to force 7. In the evening, the strain on the system had increased so that we had to heave in the paravanes by 15 m and some of the data cable to release tension.

Saturday, 20.4.2019

Surveying continued until 13:30. Then the data cable to be replaced which took until 17:30. Then surveying continued while the wind abated.

Sunday, 21.4.2019

We reached the final planned waypoint of the 3D cube in the early morning and began to fill in the gaps in the fold map.

Monday, 22.4.2019

We continued shooting infill lines without any problems.

Tuesday, 23.4.2019

We continued shooting infill lines until the last possible moment on Tuesday at 1 pm. Unfortunately there were still some gaps in the fold map. Recovery of the system took about 1.5 hours. Afterwards we started to release the ocean bottom seismometers. The first was up on deck at 4:15 pm. As two of the first four OBS came up upside down, we judged that it was too risky to recover the remaining six OBS at nighttime, because neither the strobe lights nor the radio beacon would work. Therefore, we ran multi-beam and Parasound profiles during the night and postponed recovery of the remaining OBS until Friday morning.

Wednesday, 24.4.2019

At break of dawn we released the 5th OBS which responded and surfaced. Just as the first and fourth OBS this one surfaced upside down confirming that the new design of the OBS is deficient and justifying our decision not to collect further OBS during night time. The remaining OBS were recovered until 10 am. Then we conducted another SVP cast for multibeam calibration and continued surveying with EM122 and Parasound to map the most recent deposits around Montserrat before finishing the science program at 21:00 and steaming towards Point a Pitre where we docked on Thursday morning at 6 am.

5 Preliminary and Expected Results

5.1 Seismic data acquisition

5.1.1 High-resolution 3D seismic imaging (P-Cable)

High-resolution 3D seismic data was acquired with the P-Cable system in the region south east of Montserrat, covering parts of the mass transport complex SE of Montserrat and almost the entire southern Kahouanne seamount. To image the region of interest, a NW-SE-striking survey area of 13 km by 3.5 km was planned with sail lines spaced 70 m apart.

5.1.1.1 System setup

5.1.1.1.1 Seismic Source

During the seismic experiment two GI-Guns were used in true GI mode as seismic source. Both guns were connected with a stringer hanging on two chains about 1 m beneath the guns. Two buoys stabilized the guns in a horizontal position at a water depth of ~1-2 m. Each GI gun comprised of 105 in^3 generator and 105 in^3 injector chambers. An unfiltered frequency spectra of one shot during the P-Cable survey is shown in figure 5.1. A gun hydrophone provided both the time break and the shape of the near-field signal for permanent monitoring and quality control of the source signal. Due to display problems in the gun controller, the release of the injector pulse was triggered with a delay of 25 ms with respect to the generator pulse. This delay value was

adopted for an approximate source depth of 1 m and a gun pressure of 160 bar. We estimated a delay of -27 ms from the acquired seismic data. The shooting interval was adjusted to 5 seconds, resulting in a shot point distance of 11.25 m with a ship's speed of approximately 4.5 knots in water.

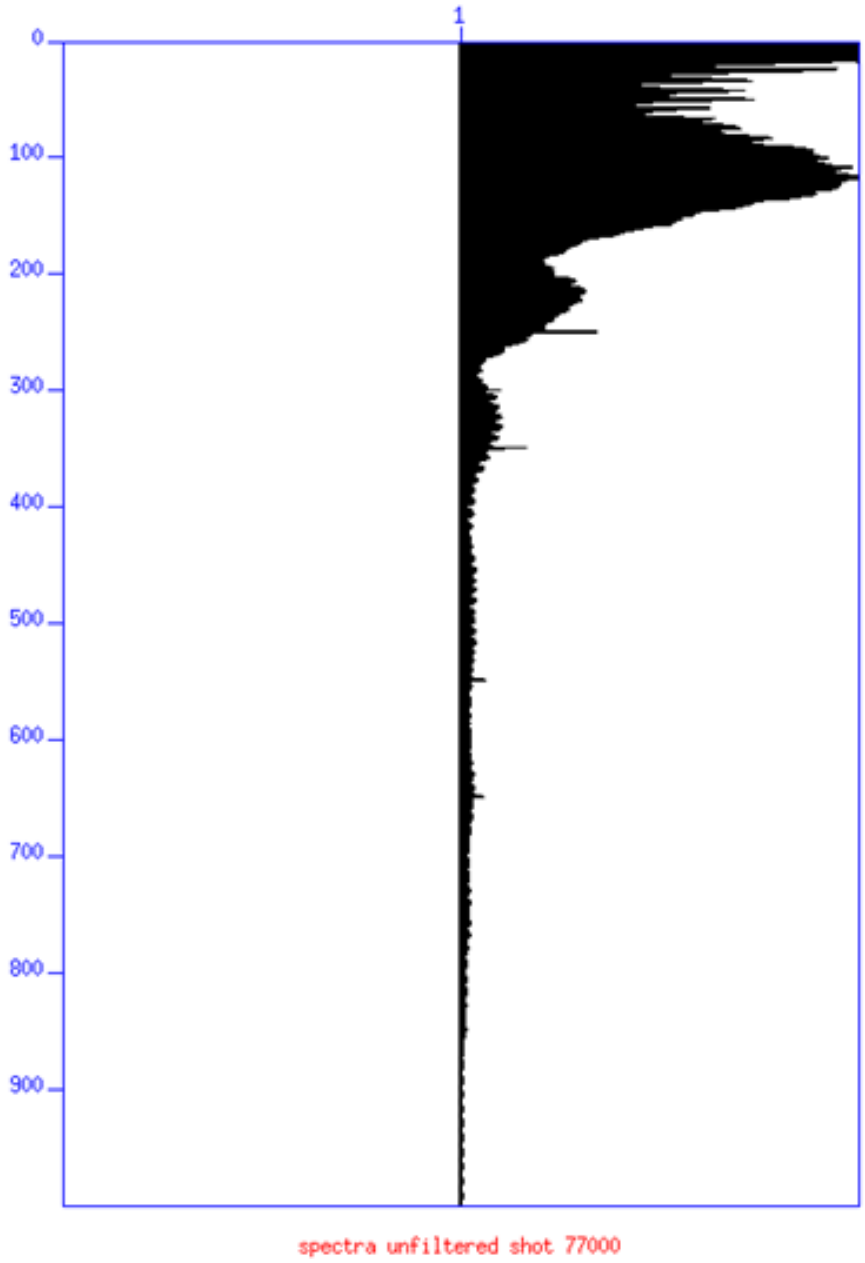

Fig. 5.1: Unfiltered frequency spectra of one shot during the P-Cable survey.

5.1.1.1.2 Streamer setup

Each active streamer section contained 8 hydrophones with a group spacing of 1.56 m. Each section had an analog-to-digital (AD) converter module, connected to the junction boxes on the cross cable via a 5 m long lead-in cable. Communication between the cross cable and the recording system in the lab was established via TCP/IP protocol. The streamer power supply unit in the lab managed the power supply and communication between the recording system and the AD digitizer modules.

5.1.1.1.3 Data recording

Data were recorded with acquisition software provided by Geometrics. The analogue signal was digitized with 2 kHz. The seismic data were recorded as multiplexed SEG-D. Recording length was 4 seconds. One file with all channels within the streamer configuration was generated per shot. The corresponding logged shot file reports shot number and time information contained in the RMC string. The acquisition PC allowed online quality control by displaying shot gathers, a noise window, and the frequency spectrum of each shot. The cycle time of the shots were displayed as well. The vessel's GPS was simultaneously logged in the RMC string along with logged time and position information.

5.1.1.1.4 P-Cable Setup

We deployed a 199 m long cross cable with 16 streamers attached (Fig. 5.2). The outer three streamers on each side of the cross cable were spaced approx. 14 m apart and the inner ten were spaced approx. 9 m apart. Spherical floats were attached to each junction box, except those at the outermost streamers (streamers 1 and 16). Additionally, single floats were tied to the cross cable between the following streamers: 6, 7, 8, 9, 10 and 11. These provided additional buoyancy in the center of the cross cable where most sag was expected. The system consisted of oil filled streamers and solid state streamers. The paravanes were towed with 96 m of trawl wire rolled off the winch in order to improve the spread of the system. GPS receivers were attached to each paravane and to a known position on the ship for reference.

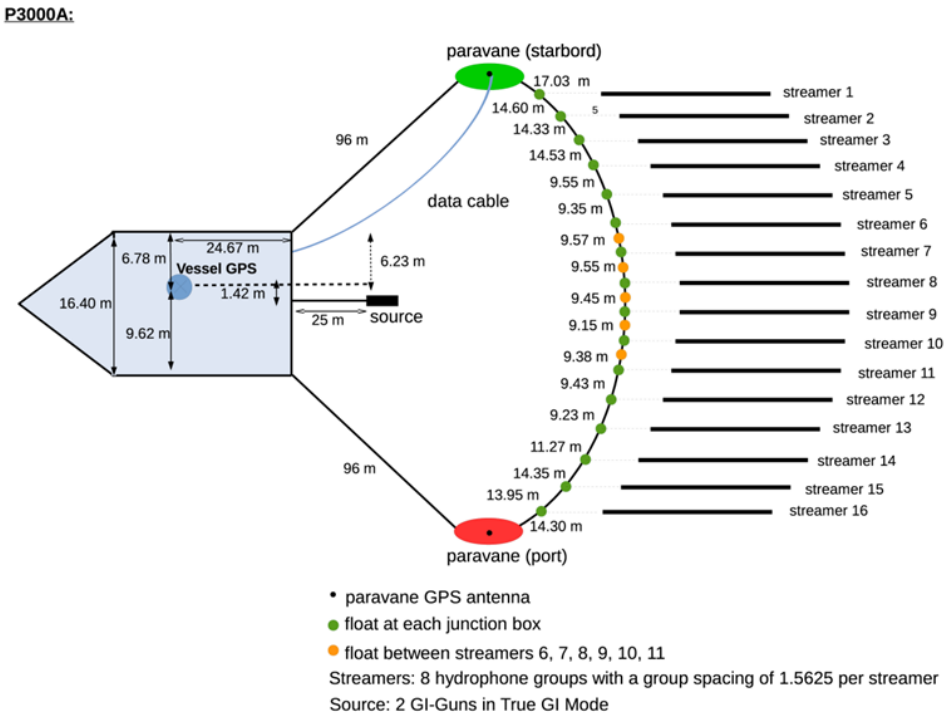

Fig. 5.2: P-Cable configuration after first deployment.

After ~22000 shots streamers 2 & 8 could not be detected anymore, therefor the setup changed to the geometry shown in figure 5.3.

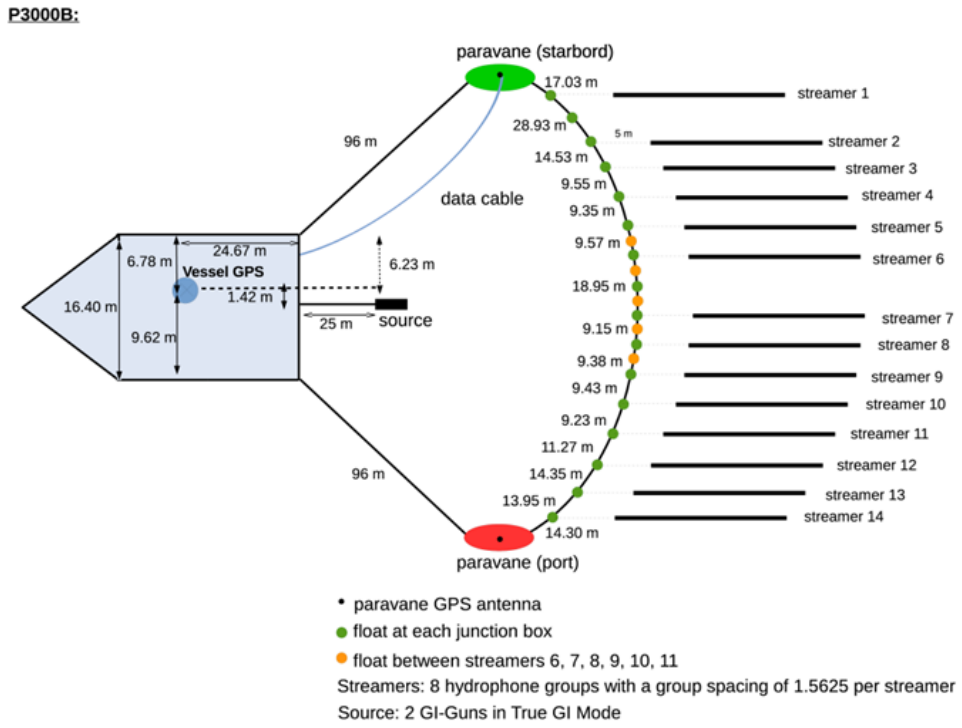

Fig. 5.3: P-Cable configuration after second deployment. Streamer segments 2 & 8 were not connected anymore.

After 55000 shots the cross cable was damaged by moored fishery equipment and had to be replaced (Fig. 5.4). After the replacement all 16 streamers were detected by the acquisition software.

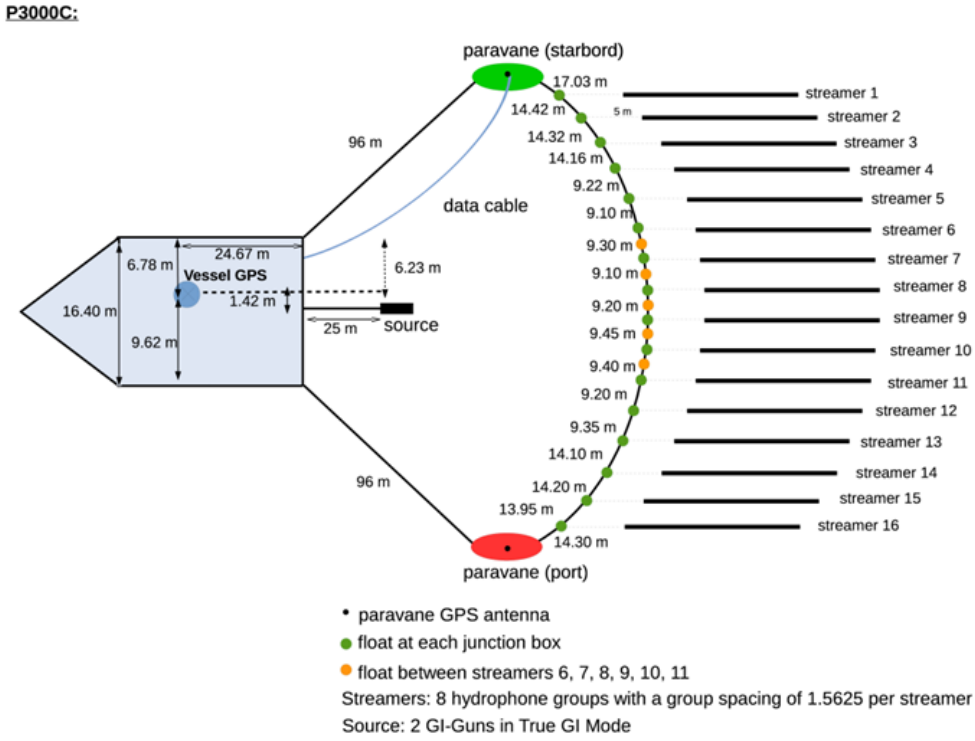

Fig. 5.4: P-Cable configuration after third deployment.

Due to technical issues regarding the data cable, the cross cable had to be pulled closer to the ship after 57000 shots and even closer after 75000 shots (approx. 85m offset between ship and each paravane). The broken data cable was replaced after 86000 shots and the offset between ship and paravanes was increased to back to 96m.

5.1.1.2 Preliminary results

On-board processing included predictive positioning of the streamers from the paravane locations under the assumption that the cross cable conforms to a catenary curve as it is towed through the water. From the seismic data a delay of -27 ms was evaluated. The source-receiver locations were binned on a grid with 6.25 m by 6.25 m cells resolving in good fold coverage (Fig.5.5 left). Seismic traces were then balanced and filtered (Fig. 5.5 right). The NMO correction was run with a constant velocity of 1511.32 m/s derived from SVP measurements and the data were stacked. The stacked data were then interpolated and migrated in two passes (first cross-line then in-line) with a 2D Stolt algorithm (1500 m/s constant velocity model).

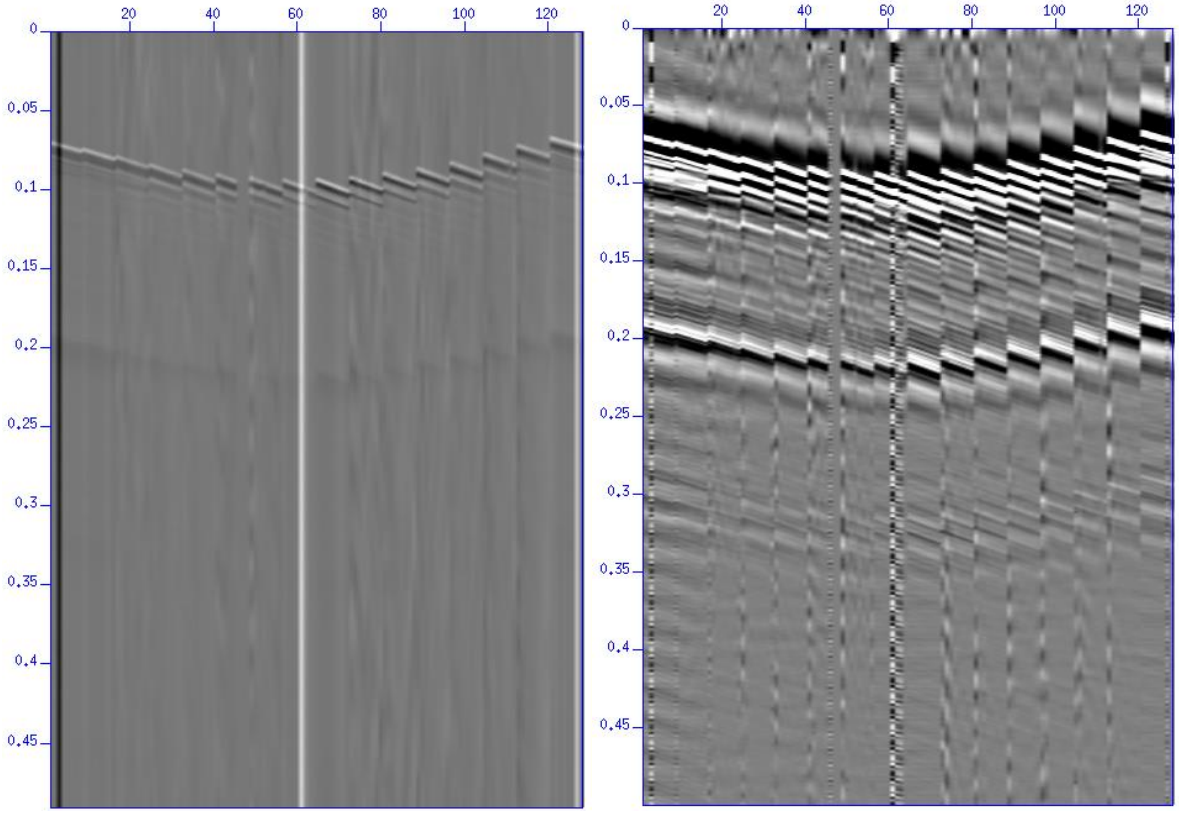

Fig. 5.5: Unfiltered shotgather of one shot during P-Cable survey (left) & filtered shotgather with corner frequencies at 25, 45, 340, 500 Hz (right).

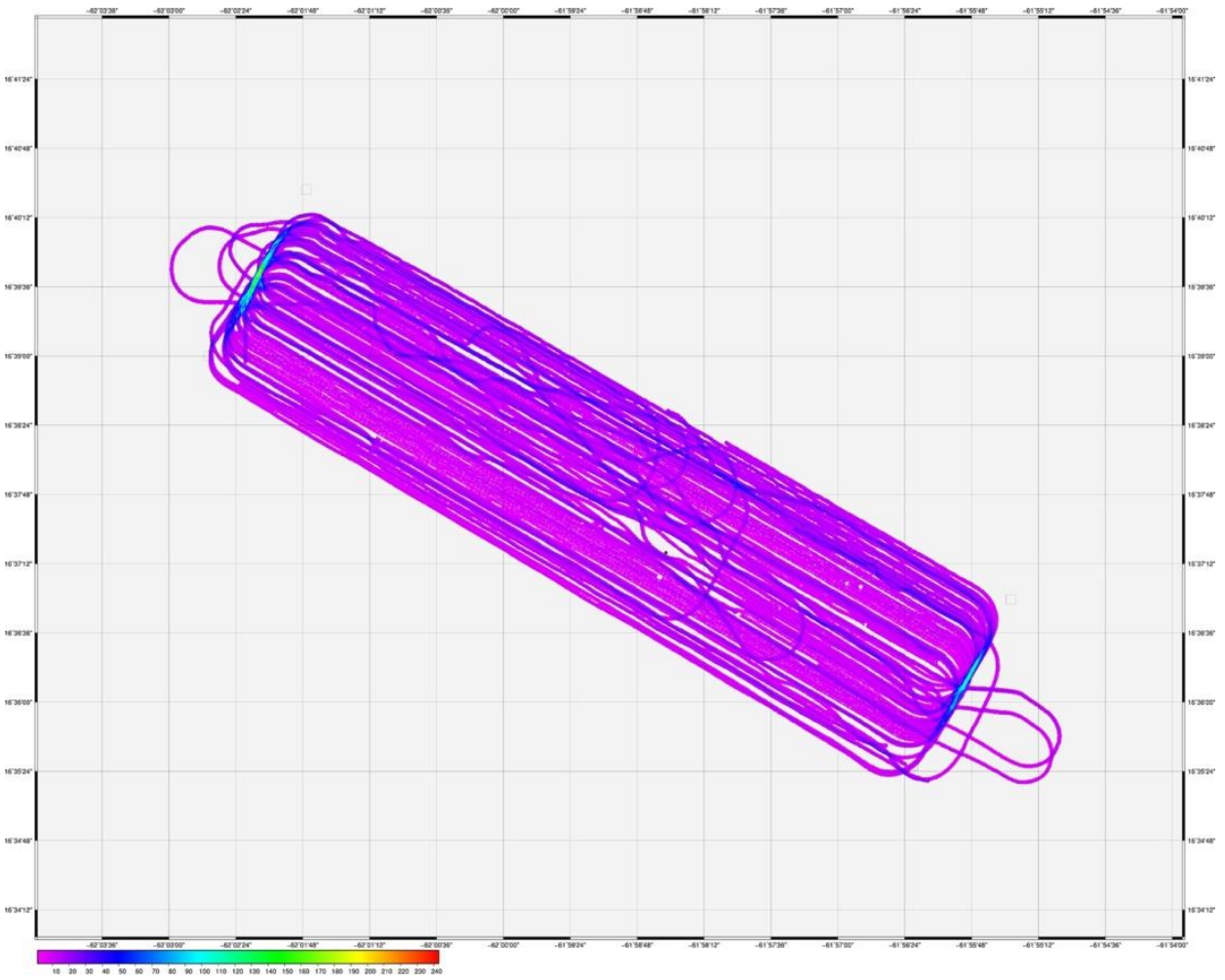

Fig. 5.6: Foldmap of the acquired 3D seismic cube. White gaps are due to moored fishery equipment within the area and strong currents.

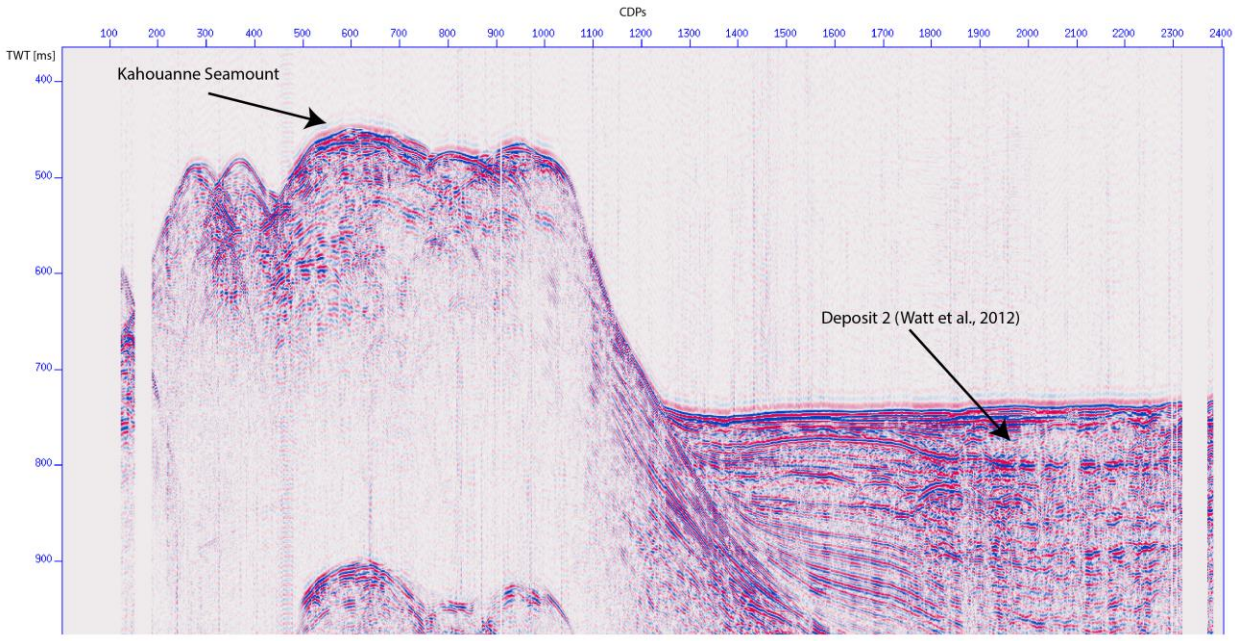

Fig. 5.7: Stacked inline of the 3D seismic cube. Due to partly insufficient fold, gaps can be observed at the edges of the profile.

The P-Cable 3D seismic data image a part of the central and distal deposit of the Montserrat flank collapse and the adjacent southern Kahouanne seamount. The on-board processing was rather difficult due to the gaps in the cube and the short time after finishing the survey. We managed to give over a preliminary migrated cube to the next leg (M154/2) to give them the best knowledge in order to find the best locations for drilling into and trough the different deposits. Our first results show that the 3D data can resolve the different failure deposits and we are positive that a further interpretation in 3D will allow to verify a) if deposit 2a and 2b origin from one event, b) if deposit 2b eroded into deposit 2a or c) if blocks from deposit 2a extent into deposit 2b. As the so-called deposit 2 runs up on the flank of the Kahouanne seamount in the measured area we expect that the 3D mapping of this structure will allow to determine the initial velocity of the material.

The part of the P-Cable data that covers the Kahouanne seamount shows that its flanks are well layered and undisturbed. Post cruise migration of the data in 3D and further interpretation will give new insights on the internal structure of the volcano.

5.1.2 2D seismic imaging

5.1.2.1 System setup

High resolution 2D seismic data (Fig. 5.8) was acquired in advance to the deployment of the P-Cable system, during P-Cable maintenance and during an OBS shooting survey after the OBS deployment. Overall, we shot three different 2D seismic surveys with four different acquisition configurations.

The configuration of the GI-Gun as well as the data recording was similar to the 3D survey.

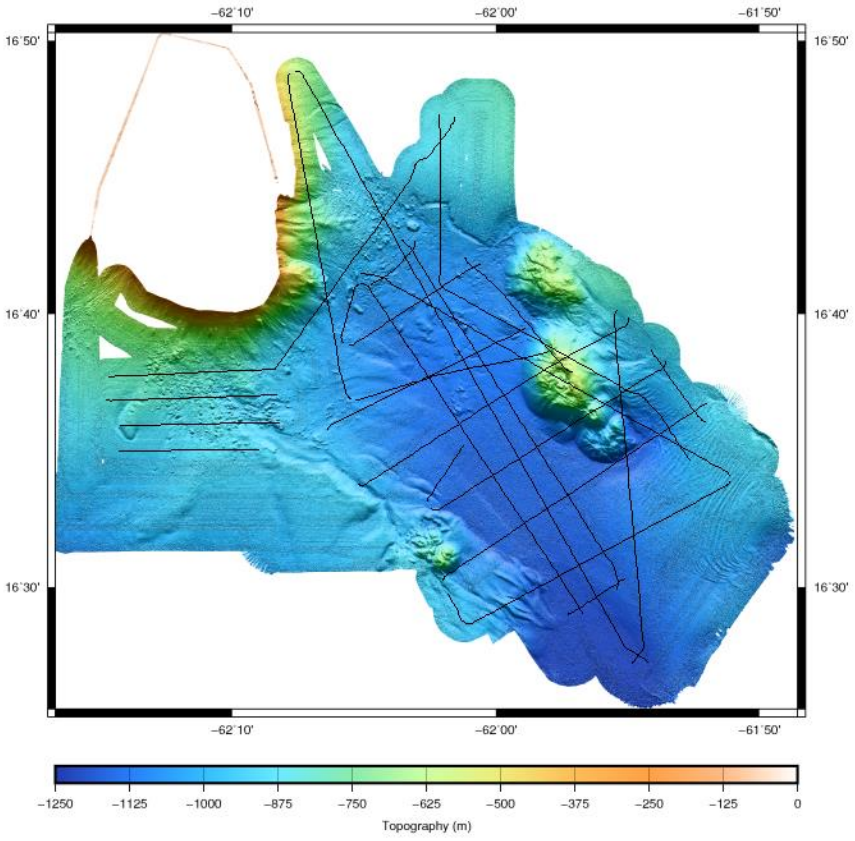

Fig. 5.8: Map of the entire processed 2D seismic.

5.1.2.1.2 Streamer setup

We used different configurations of digital streamer length (Geometrics GeoEel streamer segments) for recording the seismic signal. Deck geometries, streamer configuration and seismic gun setting for the 2D survey are illustrated in figure 5.9. The seismic recording unit consists of a tow cable, one 25 m long vibro-stretch section behind the tow cable and 2 to 7 active sections (each 12.5 m long) attached behind the stretch zone. The tow cable had a length of 31-40 m behind the vessel's stern. Each active section contained of 8 hydrophones with a group spacing of 1.56 m. Each active streamer section had an analog-to-digital (AD) converter module. The AD digitizer is a small Linux computer. Communication between the AD digitizer modules and the recording system in the lab was transmitted via TCP/IP protocol. A repeater was located between the deck cable and the tow cable (Lead-In). The streamer power supply unit managed the power supply and communication between the recording system and the AD digitizer modules. A small buoy was attached to the tail swivel of the 2D streamer.

Two Bird Remote Units (RUs) were deployed on the streamer during surveys P1000 & P5000. The RUs have adjustable wings that were controlled from the seismic lab. Controller and RUs communicate via communication coils nested within the streamer. A twisted pair wire within the deck cable connects controller and coils.

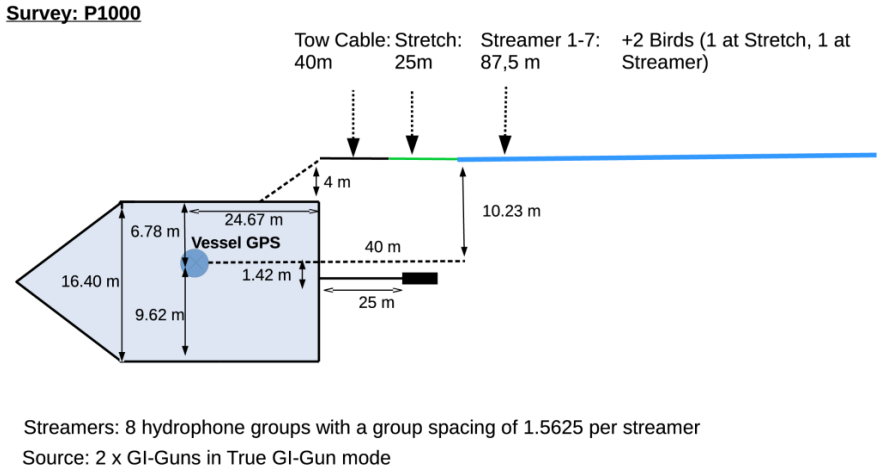

Fig. 5.9: Acquisition configuration for the first 2D seismic survey P1000.

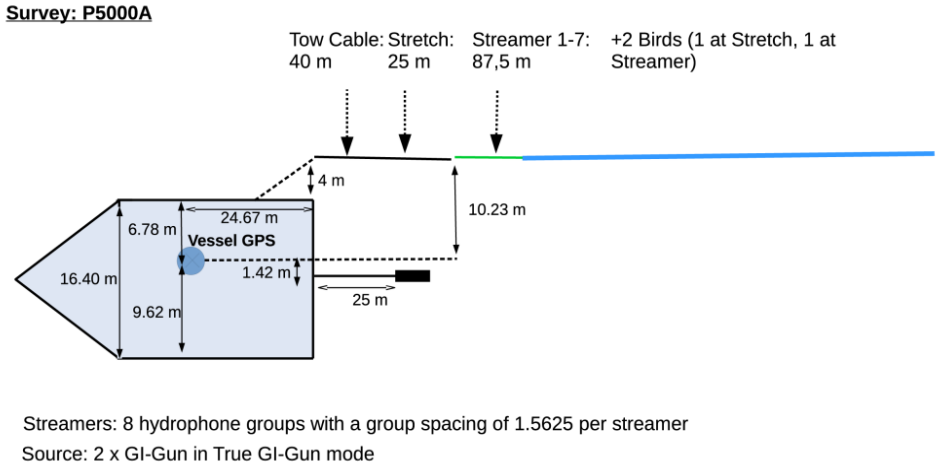

Fig. 5.10: Acquisition configuration for the second 2D seismic survey P5000A.

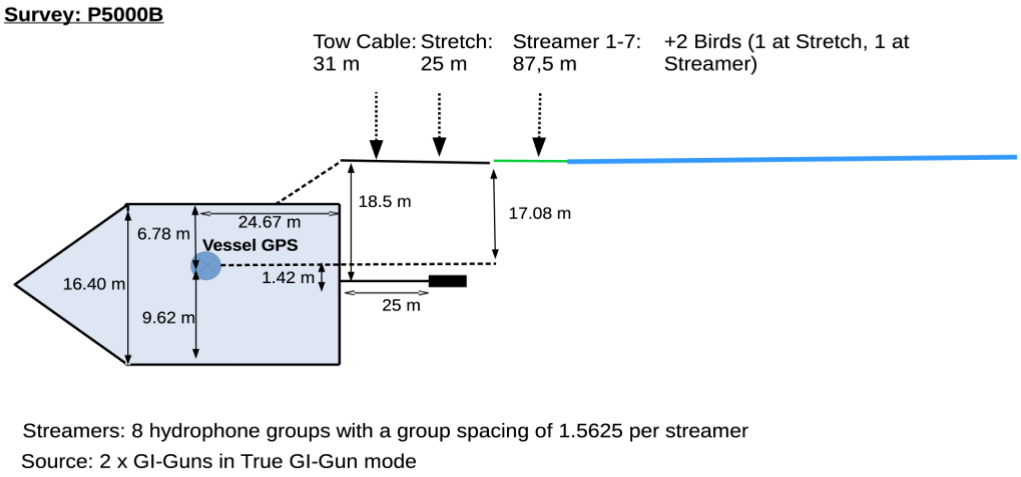

Fig. 5.11: Acquisition configuration for the second 2D seismic survey P5000B. Due to bad weather the tow cable had to be towed deeper, resulting in a geometry change.

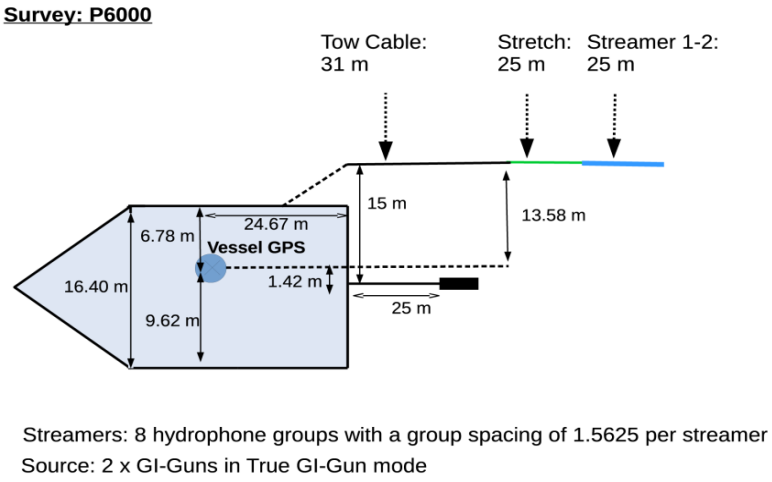

Fig. 5.12: Acquisition configuration for the third 2D seismic survey P6000.

5.1.2.2 Preliminary results

On-board processing included streamer geometry configuration, delay calculations and source and receiver depth control. From the seismic data a delay of -20 ms was evaluated. A receiver ghost effect in the seismic data could not be detected. The source-receiver locations were then binned with a common-midpoint bin spacing of 1.5625 m. Different filter tests were performed and the frequency spectra were analyzed. Seismic traces were balanced and filtered using a bandpass filter with corner frequencies at 30, 50, 420, 500 Hz. Subsequently, a normal move out correction (with a constant velocity of 1511.32 m/s derived from SVP measurements) and stacking were applied. The stack was migrated with a 2D Stolt algorithm (1500 m/s constant velocity model).

Due to technical problems with the GPS system, the survey P1000 was not processed aboard the vessel.

The high resolution 2D seismic reflection data resolve very well the near and far field of the volcanic island landslide deposits southeast of Montserrat. In the area between the island of

Montserrat and the Kahouanne seamounts the data reveal several chaotic facies that indicate a long history of multiple debris flows. Weather all deposits originate from Montserrat or to some extent from the Kahouanne seamounts will be part of the post cruise interpretation.

In addition to the image of the landslide deposits, the dataset covers parts of the southern Kahouanne seamount (Fig. 5.13). Already the 2D data show that the flanks of the seamount contain of continuous layers, which has to be further investigated in the 3D data. One explanation could be that the nature of the volcanism of the seamount is similar to Ritter Island which showed similar characteristics in the seismic images and contains of well-bedded scoriaceous deposits (Watt et al., 2019).

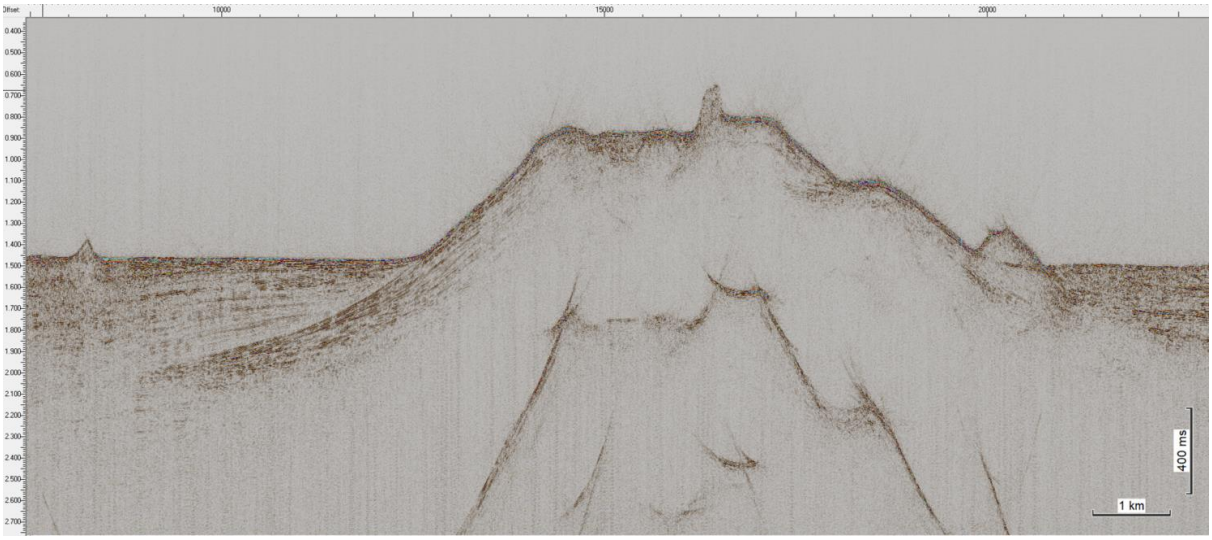

Fig. 5.13: Profile P5007 from north west to south east crossing the southern Kahouanne seamount with well stratified flanks and the chaotic volcanic island landslide deposits.

The distal 2D profiles in the south of the study area cross the Bouillante-Montserrat graben and image the normal faults that has been documented in other parts of the working area in previous studies (e.g. Watt et al., 2012; Crutchley et al., 2013). In the distal part of the landslide deposits the south-north-running profile P5017 shows the different offsets and variable density of the normal faults (Fig. 5.14).

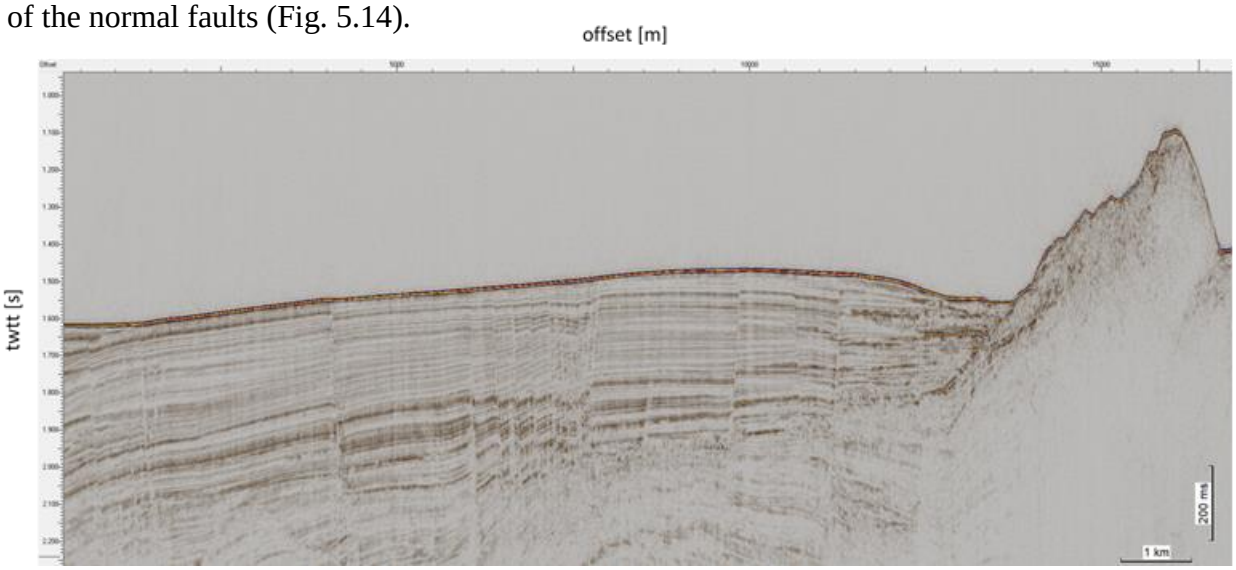

Fig. 5.14: Profile P5017 from south to north in the distal part of the landslide deposits with the very southern part of the Kahouanne seamount B.

5.1.3 Ocean bottom seismometers

5.1.3.1 System setup

A total of 10 short-period Ocean Bottom Seismometer (OBS) instruments provided by the GEOMAR pool were available for deployment during cruise M154/1. The GEOMAR OBS consists of four floats, which are connected to a frame and is generally equipped with a three-component seismometer, a hydrophone and a data recorder encased in a high-pressure tube (Fig. 5.15). The sensors are *HTI-01-PCA* hydrophones from High Tech Inc. The sensitive seismometer is clamped between the anchor and the OBS frame, which allows for optimal coupling with the sea floor. The three-component seismometer (K.U.M), usually used for active seismic profiling, is housed in a titanium tube. Geophones of 4.5 Hz natural frequency were used during M154/1. The recording devices were GEOLOG loggers developed at GEOMAR sampling at 500 Hz. The recorders require reduced power consumption with increased bandwidth for the hydrophone component and an autonomous time signal based on an atomic clock, which was synchronized before the deployment. The floatation is made of syntactic foam and is rated, as are all other components of the system, for a water depth of 6000 m. While deployed at the seafloor the entire system rests horizontally on the anchor frame. The instrument is attached to the anchor with a release transponder. The release transponder is the *K/MT562* made by K.U.M GmbH. Communication with the instrument for release and range is possible through a transducer hydrophone, which is lowered ~10 m into the water. Release and range commands are successful up to ranges of 5 miles. After releasing its anchor weight of approximately 60 kg, the instrument ascends to the surface with the floatation on top. This ensures a maximally reduced system height and water current sensibility at the ground (during measurement). On the other hand the sensors are well protected against damage during recovery and the transponder is kept under water, allowing permanent ranging, while the instrument floats to the surface.

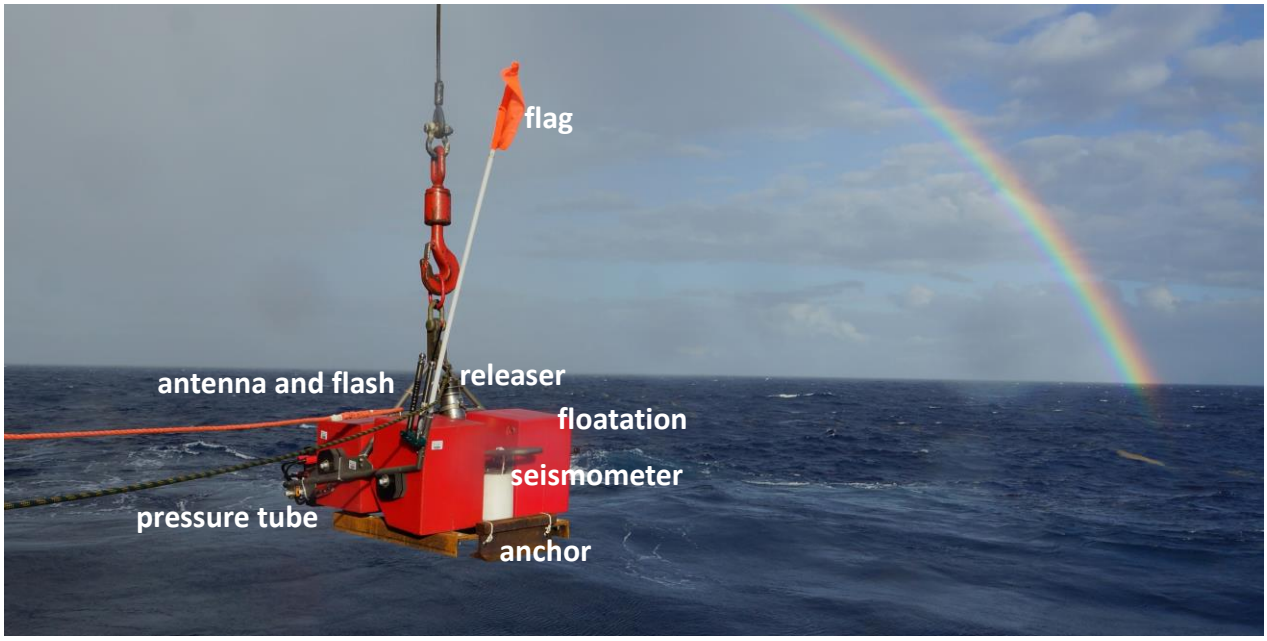

Fig. 5.15: Ocean Bottom Seismometer during the deployment (Photo S. Kontradowitz).

A total of 10 OBS were deployed along the two P-Cable cubes on April 10th 2019. The water depth varied between 1080 m and 1180 m. Afterwards, the airgun and the P-Cable System were deployed and one 3D cube was collected. Additionally, some 2D profiles, in some cases with some streamer segments, were collected.

All 10 OBS were recovered successfully on April the 23rd and 24th and the recorders were synchronized.

5.1.3.2 Preliminary results

The main target of the OBS experiment was to provide seismic velocity information for the multi-channel seismic processing. All data have been copied and converted to Pseudo SEGY. A first quick quality control showed promising data, but a detailed processing will be done after the cruise in Kiel (Fig. 5.16).

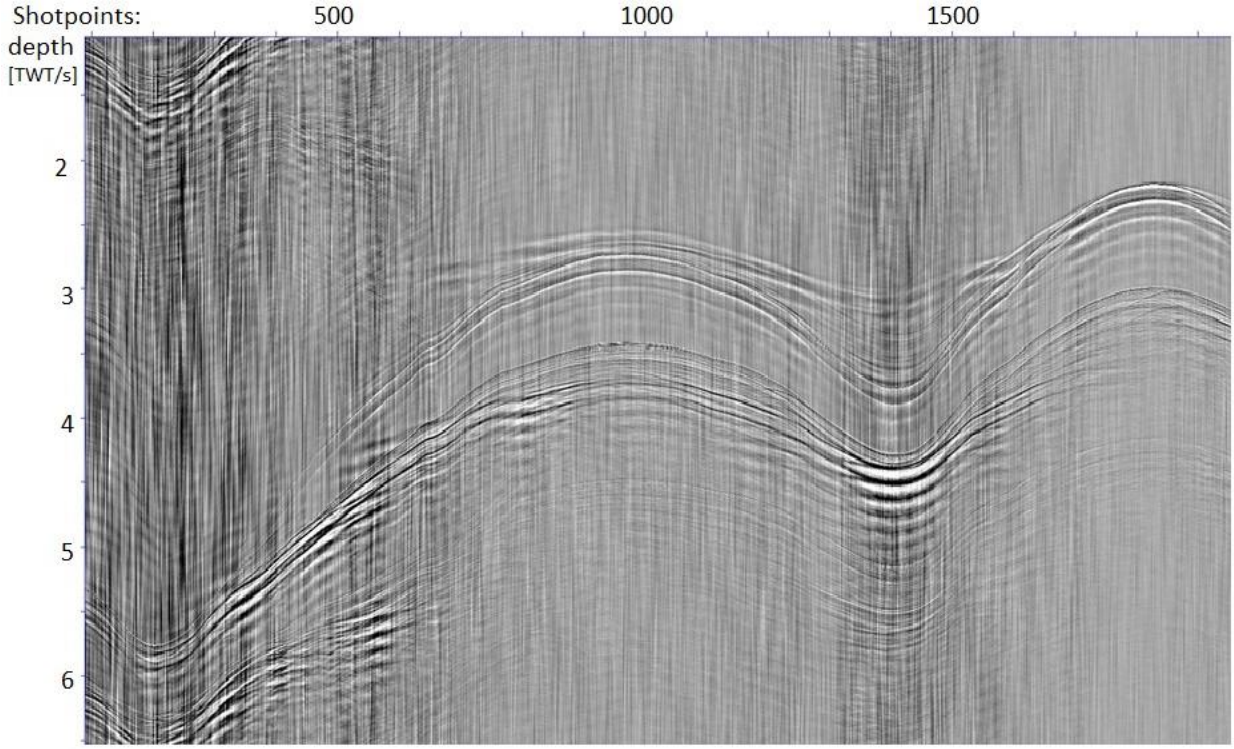

Fig. 5.16: Data example of hydrophone record section of OBS02.

5.2 Underway Hydroacoustics

5.2.1 Equipment and Method – Multibeam Bathymetry

RV METEOR is equipped with two Kongsberg Maritime multibeam echosounder. The EM122 system operates at 12 kHz and covers water depths from 20 meters below the transducers up to full ocean depth; while the EM710 system offers a frequency range from 40-100 kHz of signals for water depths ranging from 3 m below transducers to roughly 1000 m. Two different transmit pulses can be selected: a CW (Continuous Wave) or FM (Frequency Modulated) chirp. The sounding mode can be either equidistant or equiangular or mixed, depending on operation preferences and requirements. Both systems can be operated in single-ping or dual-ping mode, where one beam is slightly tilted forward and the second ping slightly tilted towards the aft of the

vessel. The whole beam can also be inclined towards the front of the back and the pitch of the vessel can be compensated dynamically. The EM122 system produces 432 beams covering a swath angle of up to 150° while the EM710 system produces 432 beams for a maximum swath angle of 140°. Both systems offer a high-density beam-processing mode with up to 800 soundings per swath. The swath angle, however, can be reduced, if required.

The transducers of both multibeam echosounder systems of RV METEOR are mounted in a so-called Mills cross array, where the transmit array is mounted along the length of the ship and the receive array is mounted across the ship. The system on RV METEOR is of a 1° x 2° design. The EM712 system installed on RV METEOR is of a 1° x 1° design, but transducers are much smaller.

The echo signals detected from the seafloor go through a transceiver unit (Kongsberg Seapath) into the data acquisition computer or operator station. In turn, the software that handles the whole data acquisition procedure is called Seafloor Information System (SIS). In order to determine the point on the seafloor, where the acoustic echo is coming from, information about the ship's position, movement and heading, as well as the sound velocity profile in the water column are required. Positioning is implemented onboard RV METEOR with conventional GPS/GLONASS plus differential GPS (DGPS) by using either DGPS satellites or DGPS land stations resulting in quasi-permanent DGPS positioning of the vessel. These signals also go through the transceiver unit (Seapath) to the operator station. Ship's motion and heading are compensated within the Seapath and SIS. Beamforming also requires sound speed data at the transducer head, which is available sound velocity probe. This signal goes directly into the SIS operator station. Finally, a sound velocity profile for the entire water column can be obtained either from a sound velocity probe or from a CTD (conductivity, temperature and density) probe. The temperature (T), salinity (S) and pressure (p) data acquired by any CTD (conventional or mounted on the AUV) can be converted into sound speed by using a sound speed function C(S,T,p). During cruise M154/1, we used direct sound velocity measurements with a special profiler probe at the beginning, mid and end of the cruise.

In addition to bathymetric information, both the EM122 and the EM712 system register the amplitude of each beam reflection as well as a sidescan signal for each beam (so-called snippets). Both systems also allow recording the entire water column. The amplitude signals correspond to the intensity of the echo received at each beam. It is registered as the logarithm of the ratio between the intensity of the received signal and the intensity of the output signal, which results in negative decibel values. For each ping, EM122 records 432 backscatter intensity values while the EM710 records 432 backscatter values. The water column data correspond to the intensity of the echoes recorded from the instant the output signal is produced. All echoes coming from the water column, the seabed and even below the seabed are recorded for each beam. When the water column data of one ping is divided into a starboard and port subsets, one can produce two traces, one for each subset. Each trace is build up as a time series in which for each time the highest amplitude is selected from all beams. Then the starboard and the port traces are joint together.

5.2.1.1 Acquisition parameters and data processing

During cruise M154/1 the following settings of the Kongsberg EM122 system were used. The pulse was FM, ping mode was set to HD-equidistant, dual ping mode was set to fixed, and depth mode was set to automatic. The beam angle was reduced to 120° during most of the survey, except for survey lines close to the volcanic island and during the transit, where the maximum coverage was desired. Survey speed varied between 5 and 8 knots. Data were acquired continuously, except for OBS deployment and recovery. Acquisition parameters for the EM710 system were the same as those for the EM122, except for the beam angle, which was reduced to 100° during most surveys.

During transit EM122 data were collected despite higher ship's speed of up to 12 knots. Water column data were recorded at dedicated surveys. Three sound velocity probe casts and one XBT cast were used for water sound velocity profiles: one outside the 200 nm zone of the Cabo Verde Islands at the beginning of hydroacoustic data acquisition, a second SVP SE off the island of Montserrat at the beginning of the survey prior to OBS deployment, one XBT during the 3D P-Cable seismic survey and one SVP at the end of the cruise SE off Montserrat (Fig. 5.17).

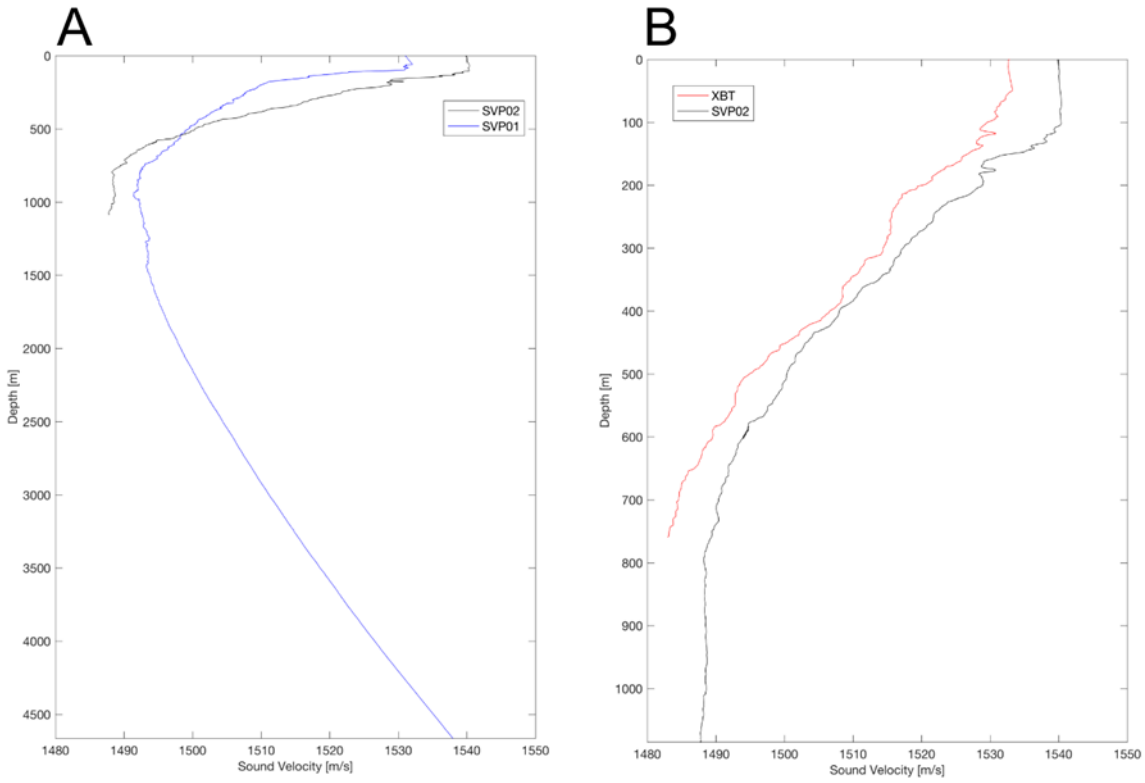

Fig. 5.17: (A) Comparison of SVP01 acquired outside the 200 nm of Cabo Verde down to ~4600 m water depth and SVP02 acquired in between Montserrat and the Kahouanne Seamounts at ~ 1100 m water depth. (B) Comparison of SVP02 and an XBT acquired during the 3D P-cable seismic survey.

Data processing has been carried out onboard using different software packages (MB Systems, QPS Fledermaus). Within MB Systems Version 5.5.2303 (release: April 28, 2017) the processing and gridding of EM122/EM710 data took place. The soundings were preprocessed from Kongsberg all-format to an internal MB Systems format (format: 59). The pings were cleaned using mbclean. First, we flagged all soundings with a deviation of 2% from the local

(N=10 pings) median. Second, we applied a swath-filter, which zaps bad rails (30 m) for each swath. Residual bad soundings or spikes were cleaned with the manual 3D ping tool (mbeditviz). The survey area is impacted by little tidal heave with ±0.15 m (Fig. 20). However, the OTPS model TPX-O8-Atlas v1 (resolution 1/30°) was used to calculate the tidal water level time series (Fig. 5.18) for correcting bathymetry (mbotps).

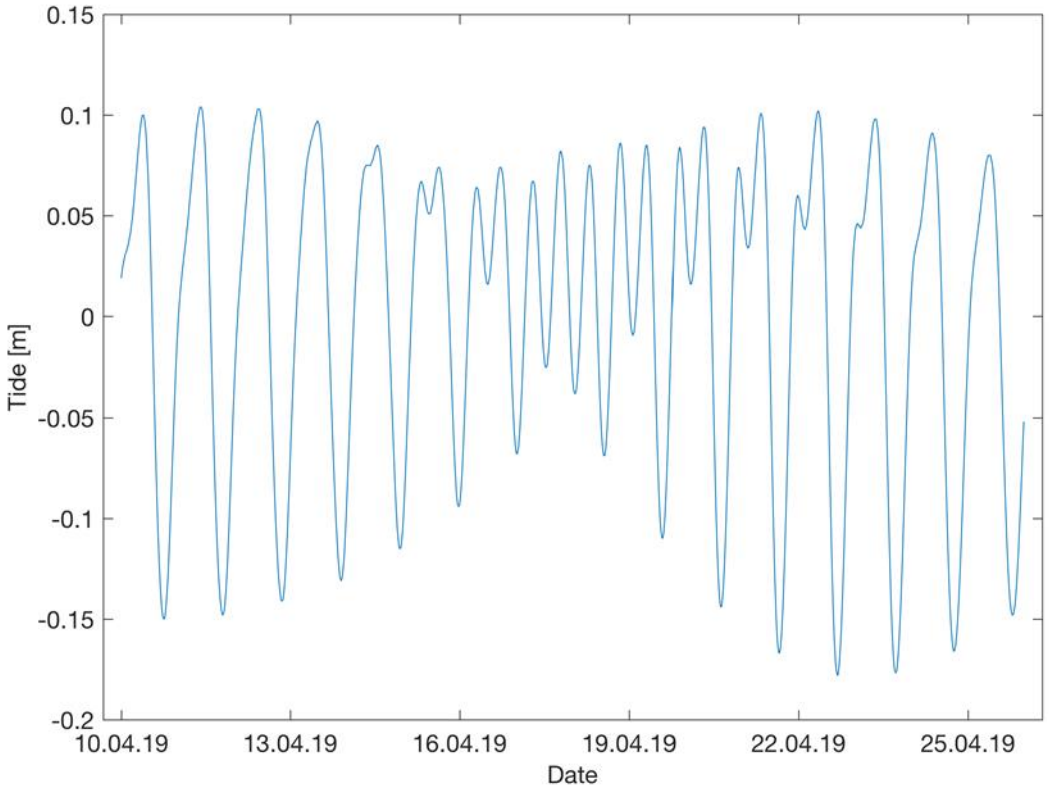

Fig. 5.18: Tidal water level during the days of the hydroacoustic surveys starting at the 10th until the 26th April 2019. The tidal water level varies only little in the survey area and therefore could be neglected given the accuracy of the EM122 multibeam system.

The data were subsequently gridded with MB-Systems using a Gaußian weighted mean with a cell size of 10-15 m, depending on the coverage and water depth. All data were interpolated for a maximum of 3-5 cell sizes (3 for 15 m grid cell size, 5 for 10 m grid cell size) to achieve good coverage for the high-resolution grid.

The backscatter (amplitude) signal is stored and preprocessed automatically by the Kongsberg software Seafloor Information System (SIS), including altitude processing, time varying gain (TVG) and angle varying gain (AVG). The backscatter have been processed using QPS FMGeocoder, where radiometric corrections, filtering, angle-varying gain and anti-aliasing filters and topographic corrections were applied to the backscatter data before outputting a georeferenced mosaic.

Both the EM122 and the EM710 multibeam echosounder produce a second type of raw data files with extension *.wcd, which stores water column data. These files were imported into QPS FMMidWater. The raw multibeam echosounder data (.all format) and associated water column data (.wcd) were placed into a single folder and imported. Each line was subsequently downsampled, opened in fan view (across track), and displayed as a curtain image (along track,

range-stack view). The data were also filtered by intensity. No evidence of backscatter anomalies, which could be indicative of fluid seepage from the seafloor, was observed in the water column data.

5.2.1.2 Preliminary results

Although multibeam bathymetry data have been recorded and edited during the entire transit in international waters only those data collected in the vicinity of the Mid-Atlantic Ridge been looked at in detail as an example (Fig. 5.19). Here, the seafloor rises towards depths of 2200 m below the sea surface and drops towards the rift axis. The backscatter intensity map shows the change of lower backscatter away from the main rift axis to high values inside the recent rift axis. The high values may be partly due to the rough terrain and may emerge from topographic effects (Fig. 5.19 C). However, the overall quality of the transit data looks promising and the chosen grid cell size of 100 m and be decreased to at least 75 m, if required.

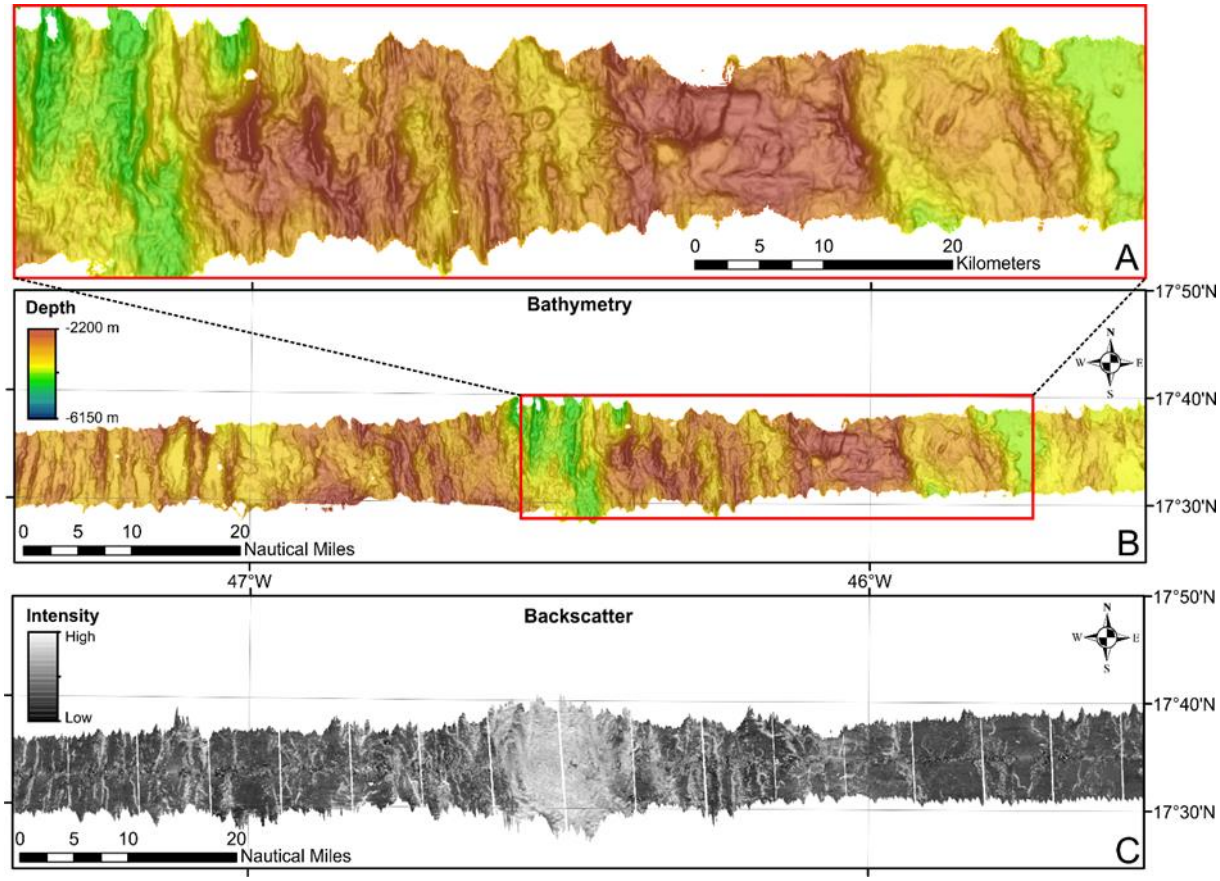

Fig. 5.19: Slope-shaded relief map of the EM122 data acquired during the transit from Mindelo (Cabo Verde Islands) towards the survey area offshore Montserrat gridded at 100 m spatial resolution. (A) Zoom of the bathymetric map showing the Mid-Atlantic Ridge and rift. (B) Bathymetric map gridded with 100 m spatial resolution showing the Mid-Atlantic Ridge and rift. (C) Corresponding backscatter intensity map of the EM122 backscatter snippet data.

The working area predominantly south of the island of Montserrat shows a basin up to 1100 m deep that is bounded by the island of Montserrat, Guadeloupe towards the south and by the Kahouanne Seamounts towards the East. The EM122 data shows good quality and high detail in

the working area comprising prominent bathymetric features off the island of Montserrat. The proximal surrounding of Montserrat is characterized by blocky, rugged seafloor morphology indicating debris avalanches in the direct surrounding of the island (Fig. 5.20). Figure 5.20 B shows the proximal part comprising blocky, hummocky seafloor morphology with prominent channels carving into the substratum. A sedimentary infill marks the eastern boundary with a channel separating the background sedimentation from the landslide material (Fig. 5.20 B). This area has been previously identified as headwall scarp with an infilled contouritic drift and moat (CITE). The Kahouanne Seamounts show a prominent morphology with a flat top and a volcanic cone (Fig. 5.20 C). The southeastern part of figure 5.20 C shows prominent sedimentary waves and an erosional channel intersecting the sedimentary waves and the Kahouanne Seamount.

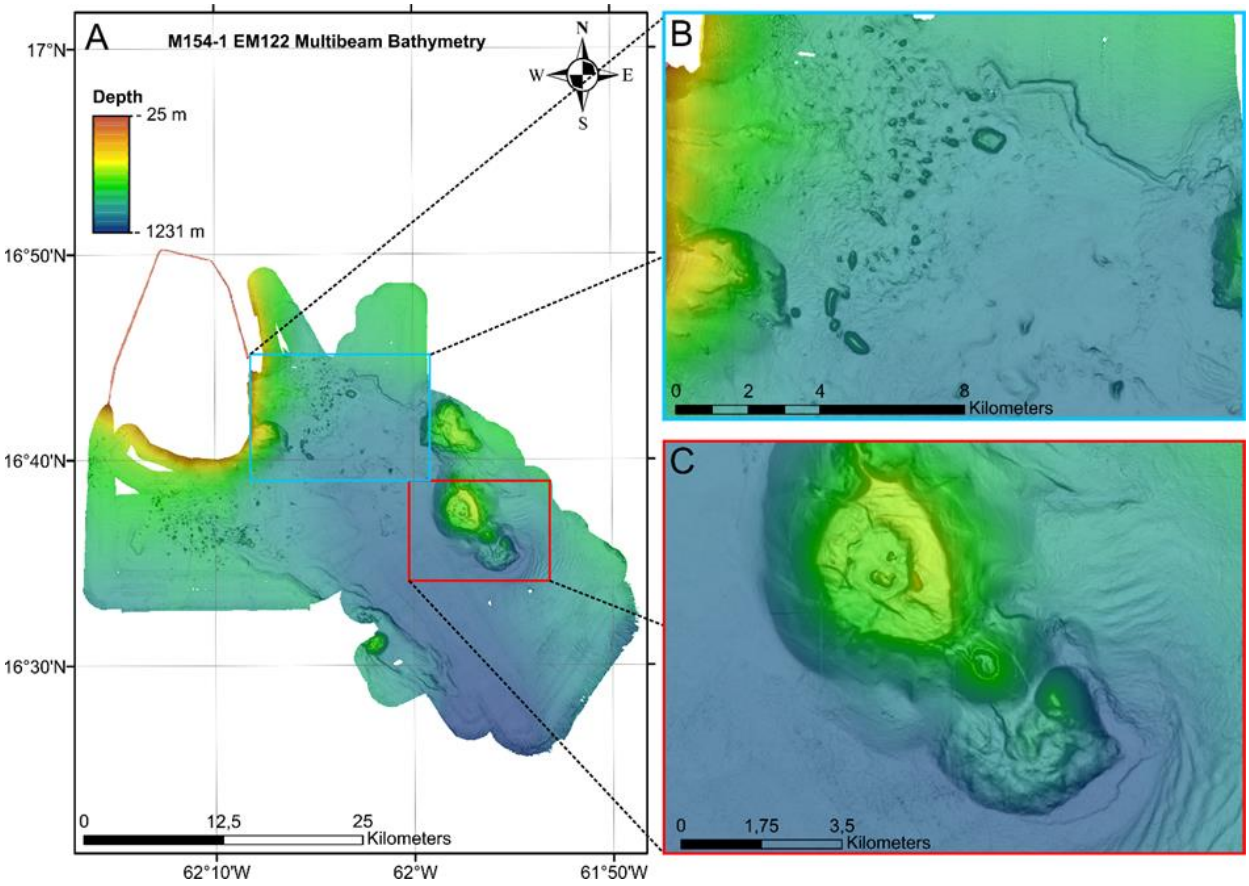

Fig. 5.20: Slope-shaded relief map of the EM122 multibeam bathymetric grid acquired during M154/1 with 15 m resolution. (A) Slope-shaded relief of all EM122 multibeam bathymetric data acquired during M154/1 gridded at 15 m resolution. (B) Zoom in of the proximal landslide area offshore Montserrat with various large blocks, contouritic depositions (moat, drift), presumably pockmarks and erosional features. (C) The southern Kahouanne Seamount with volcanic cones, faults with sedimentary waves and erosional channel towards the Southeast.

5.2.2 Parasound

5.2.2.1 Equipment and Method – Parasound

The hull-mounted parametric sub-bottom profiler PARASOUND P70 (Atlas Hydrographic) was operated on a 24-hour schedule for flare imaging and to provide high-resolution (less than

15 cm for sediment layers) information on the uppermost 50-100 m of sediment. The system has a depth range of 10 m to > 11000 m (full ocean depth) and a maximum penetration of 200 m. This high sediment penetration is acquired through the high pulse transmission power of 70 kW.

The PARASOUND P70 is a narrow beam sediment echo sounder, providing primary frequencies of 18 (PHF) and adjustable 18.5 – 28 kHz, thus generating parametric secondary frequencies in the range of 0.5 – 6 kHz (SLF) and 36.5 – 48 kHz (SHF) respectively. The secondary frequencies are obtained through nonlinear acoustic interaction of the primary waves at high signal amplitudes. This interaction occurs in the emission cone of the high-frequency primary signals, which is limited to a beam width of 4.5° x 4.5° for the PARASOUND P70. The system consists of four identical transducer modules, each about 0.3 m x 1.0 m. The P70 version includes 384 acoustic elements combined to form 128 stave channels. The resulting footprint size is approx. 4% of water depth and vertical and lateral resolution is significantly improved compared to conventional 3.5 kHz echo sounder systems. The system provides features like recording of the 18 kHz primary signal and both secondary frequencies, continuous recording of the whole water column, beam steering, different types of source signals (continuous wave, chirp, barker coded) and signal shaping. Digitization takes place at 98 kHz to provide sufficient sampling rate for the high secondary frequency. A down-mixing algorithm in the frequency domain is used to reduce the amount of data and allow data distribution over ethernet.

5.2.2.2 Acquisition parameters and data processing

For the standard operation a parametric frequency of 4 kHz (SLF) and a sinusoidal source wavelet of 3 periods were chosen to provide a good balance between signal penetration and vertical resolution. The 18 kHz signal was also recorded permanently. Within the survey area the system was mainly used for analysis of sedimentary processes, such as the identification of mass transport deposits, background sedimentation, coring locations for MeBo and tectonic surface deformation. Due to low water depth (>1500 m) within the survey area and a rugged morphology of the seafloor close to Montserrat the system was operated in a single pulse mode. Technical problems occurred rarely and could be solved during the cruise. The system was rebooted a few times due to program crashes (approx. once a week). While the rebooting-induced data gaps exceeded an hour, the overall data quality and coverage is very good.

All raw data were stored in the ASD data format (Atlas Hydrographic), which contains the data of the full water column of each ping as well as the full set of system parameters. Additionally a 200 m-long reception window centered on the seafloor was recorded in the SEG-Y and compressed PS3 data format after resampling the signal back at 12.1 kHz. This format is in wide usage in the PARASOUND user community and the limited reception window provides a detailed view of subbottom structures.

All data were converted to SEG-Y format during the cruise using the software package ps32sgy (Hanno Keil, Uni Bremen). The software allows generation of one SEG-Y file for longer time periods, frequency filtering (low cut 2 kHz, high cut 6 kHz, 2 iterations), subtraction of mean. If seismic data were collected simultaneously, one SEG-Y file was created for the length of each seismic profile. In all other cases 4h-long pieces were generated (e.g. during transit, long seismic lines). All data were loaded to the seismic interpretation software IHS Kingdom. We used IHS Kingdom to convert the subsequent SEG-Y files from amplitude to

envelope data and applied an automatic gain control (AGC) with a filter window of 0.01 s to achieve higher visibility of deeper sedimentary layers. While the AGC filtered data provides good insight on the penetration depth, the envelope data enables a better understanding of the subsurface with high- and low-reflective layers. In addition, the data were converted from time to depth domain with an average velocity of 1500 m/s to select locations for the sediment coring and get sediment thickness information. This approach allowed us to obtain a first impression of sea floor morphology variations, sediment coverage, sedimentation patterns along the ship's track, tectonic deformation and imaging of mass transport deposits.

5.2.2.3 Preliminary results

The multibeam bathymetry shows a large variety in seafloor morphology. The Parasound P70 shows overall good penetration into the subsurface, except for areas where coarse-grained, most likely volcanic material covers the seafloor, large blocks likely originating from Montserrat or steep slopes scatter the transmitted energy and distort the proper imaging of the subsurface. Overall 1109 km PARASOUND profiles have been acquired during 2D seismic, OBS and dedicated hydroacoustic surveys (Fig. 5.21 B). During the 3D P-Cable seismic survey a dense grid of total 760 km length was acquired across Kahouanne Seamounts NW towards the island of Montserrat (Fig. 5.21 A).

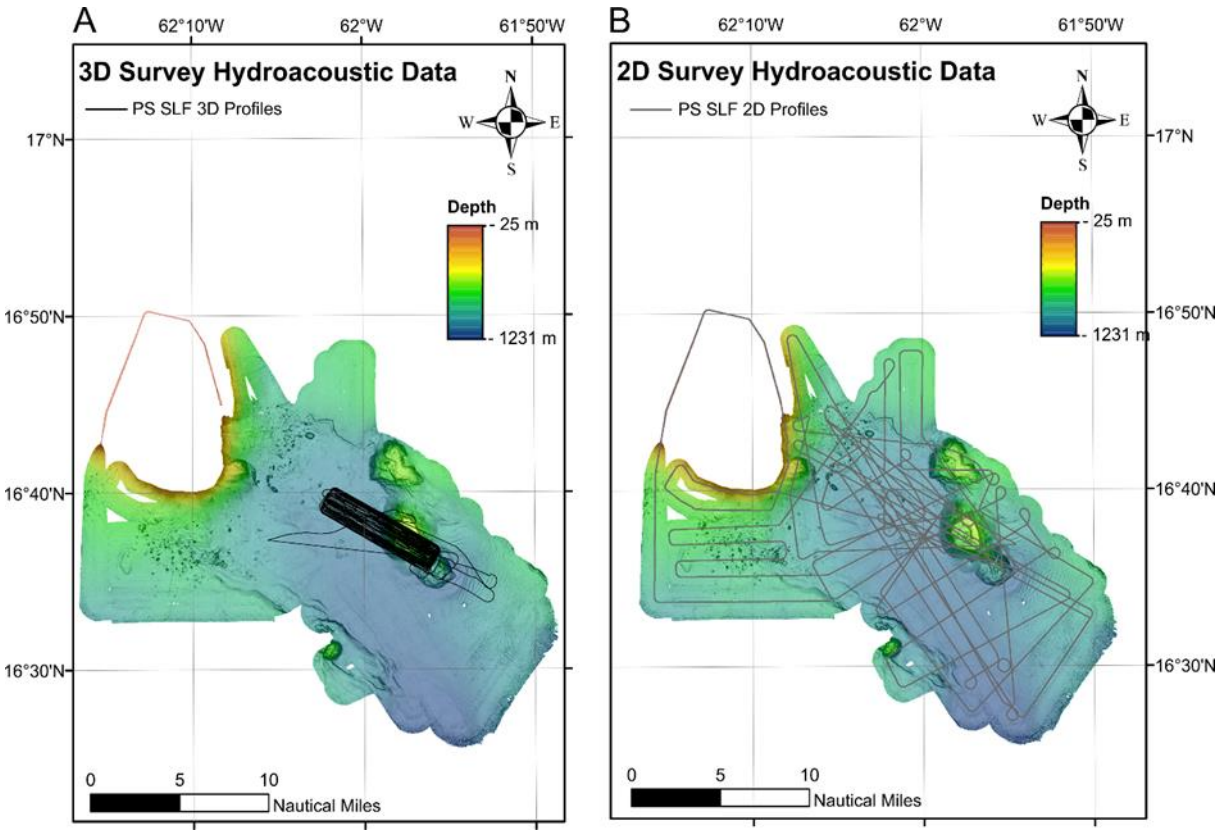

Fig. 5.21: Parasound P70 data coverage draped on EM122 multibeam bathymetric grid (15 m resolution). (A) Parasound P70 profiles acquired during 3D P-cable seismic surveys across the Kahouanne Seamount. (B) Parasound P70 profiles acquired during 2D seismic, OBS and dedicated hydroacoustic surveys.

Figure 5.22 shows Parasound P70 profile P5014, which spans 45 km from the northwestern towards the southeastern region of the working area covering major parts of the Montserrat landslide and the surrounding. The profile can be separated into proximal (Fig. 5.22 A), medial (Fig. 5.22 B) and distal (Fig. 5.22 C) from the island of Montserrat. The sub bottom profiler data shows very good penetration varying from several meters in the proximal parts to several tens of meters in the distal parts (Fig. 5.22). In areas where there are either large blocks or steep slopes, the system shows primarily the seafloor. Everywhere else, the penetration and overall data quality is sufficient to determine the processes involving sediment deposition and erosion, the transport of sediments downslope (e.g. mass transport deposits) and other geological features of the upper sedimentary succession (Fig. 5.22).

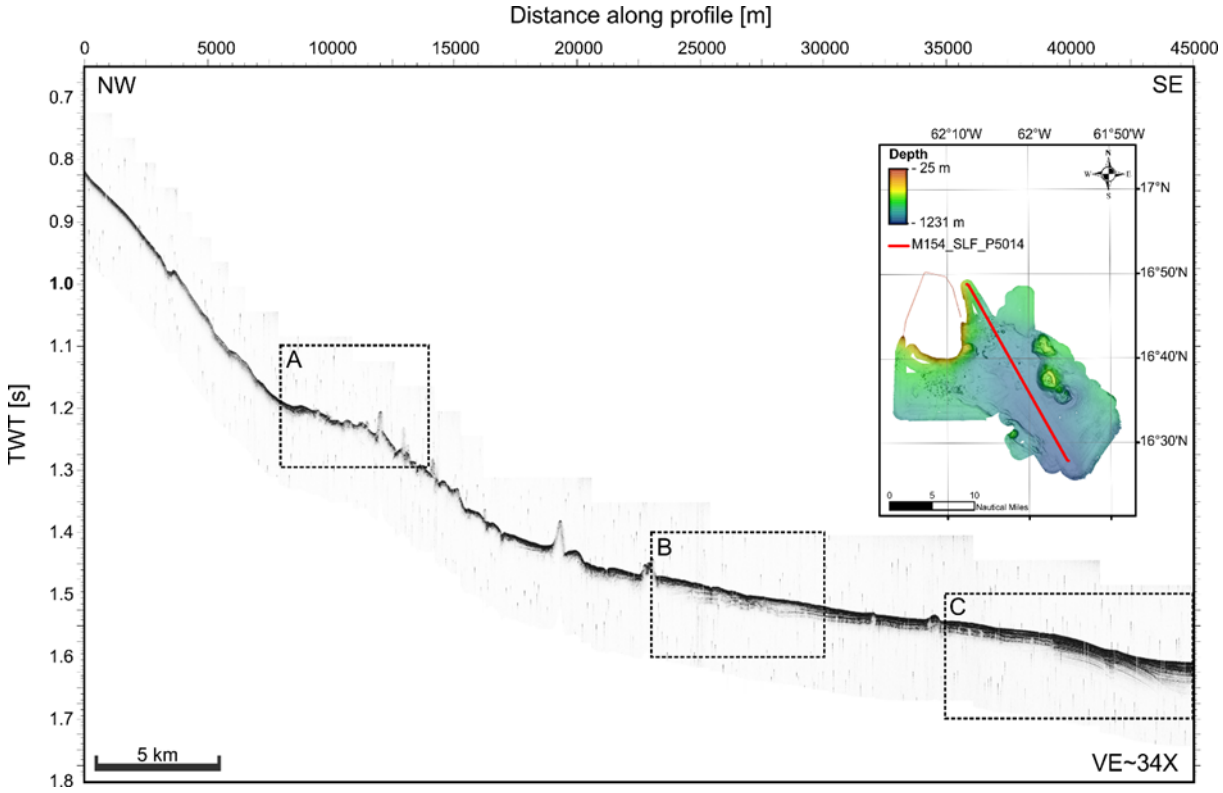

Fig. 5.22: 45-km long Parasound profile P5014 covering the proximal, medial and distal parts of the Montserrat landslides and background sedimentation in the SE part of the profile. A,B and C indicate zooms of the proximal, medial and distal parts, respectively. The profile shows two-way travel time [TWT] in seconds on the y-axis and distance along profile in meters on the x-axis.

Figure 5.22 shows three different sub bottom profiler data section of the 45-km long profile shown in figure 5.21. The data can be used to identify mass transport deposits, tectonic deformation and background sedimentation as well as the patterns of deposition and erosion in the form of contouritic deposits such as sedimentary waves or drift bodies. Figure 5.22 A shows a section of the proximal part off Montserrat, where a multitude of blocks hinders the exact imaging of the seafloor and the subsurface by inducing diffraction hyperbolas. However, the shallow subsurface is characterized by a multitude of different chaotic to transparent sediment bodies which likely represent phases of downslope mass transport. Figure 5.22 B shows the medial part of the landslide, where the shallow subsurface close the seafloor shows the same patterns of chaotic to transparent sediment bodies, similarly representing most likely downslope

mass transport deposits. These mass transport deposits show several phases (at least 3) and are varying in thickness with the thickest bodies being ~ 0.04 s TWT corresponding to ~ 30 m thickness (at 1500 m/s water sound velocity). Beneath these deposits, the sedimentary succession shows well stratified sediments with occasional folded strata. These folded strata show no thinning, indicating an in-situ folded deposition, likely above previously emplaced blocks.

Figure 25 C and CAGC show the same 10-km long profile section with two different processing flows applied. Figure 25 C shows the envelope over time, which fades into the unrecognizable with depth. Figure 25 CAGC shows the envelope data with an applied automatic gain control (Filter length 0.01 s TWT) to enhance subsurface reflection independent of their depth to a similar level. Thereby, we are able to determine the maximum penetration depth of the Parasound system, which can be traced down to ~ 0.06 s TWT corresponding to ~ 45 m below the seafloor (at constant sound velocity of 1500 m/s). We can identify the outermost extent of landslide deposit 2 (Lebas et al., 2011; Watt et al., 2012) and our data can even image well-stratified strata below the landslide deposit. The landslide seems to have stopped at a fault which emerges from the subsurface and outside of our imaging towards the seafloor, indicating the activity of the fault. Apart from the landslide history the data shows indications for dewatering processes in the form of pipe structures (zones of dimmed reflections emerging from landslide deposits towards the surface) and for tectonic deformation in the form of faults.

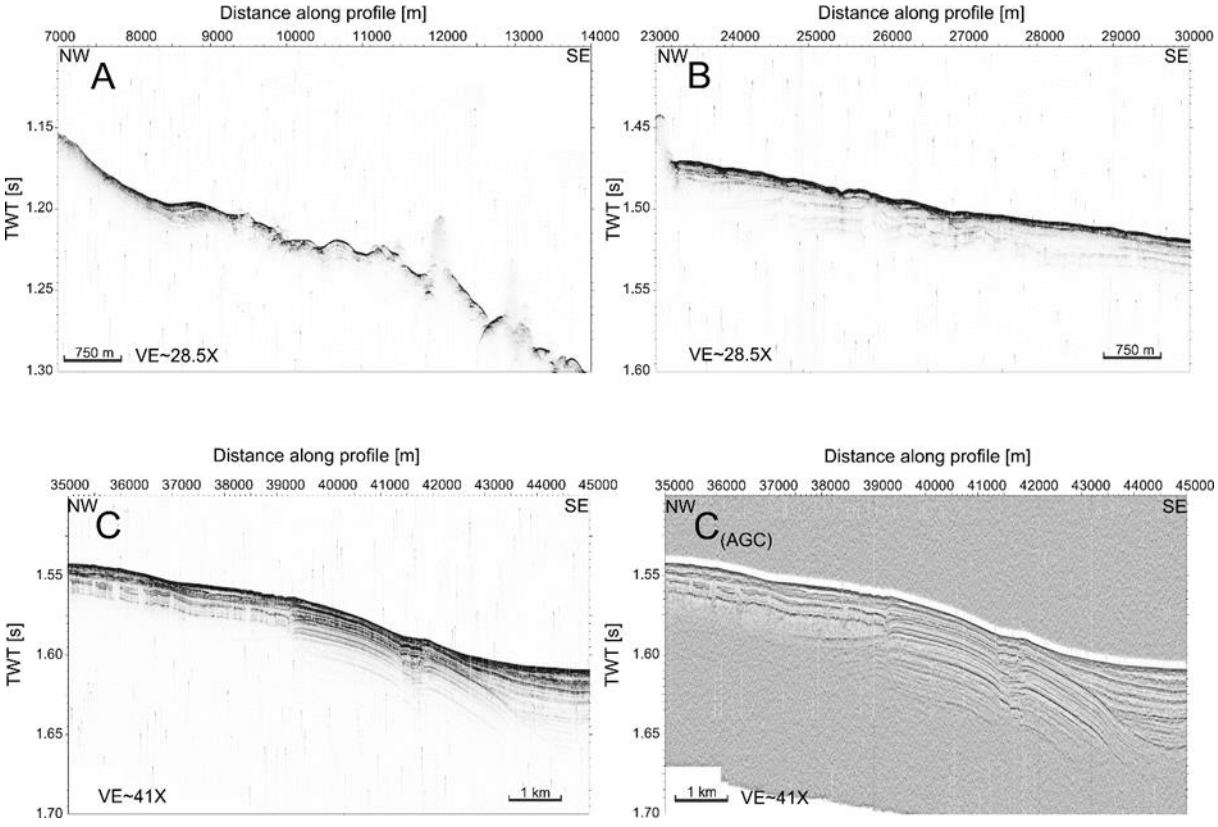

Fig. 5.23: Different sections of the 45-km long Parasound profile P5014 covering the (A) proximal , (B) medial and (C) distal parts of the Montserrat landslides. (CAGC) shows profile section C with applied automatic gain control to enhance subsurface reflections and show the maximum penetration depth (here ~ 0.06 s TWT corresponding to ~45 m at constant seismic velocity of 1500 m/s). The profiles show two-way travel time [TWT] in seconds on the y-axis and distance along profile in meters on the x-axis.

5.3 Aerosol measurements

Maritime aerosol is primarily composed of sea salt particles. However, the Sahara functions as another relevant source for aerosols over the Atlantic ocean. Storms mix sand particles into the atmosphere that may be transported by the trades across the entire Atlantic. In fact, Saharan dust constitutes a relevant nutrient source for the Amazonian rain forest. Importantly, aerosols impact the radiation budget, and thus earth's climate. This happens on the one hand via a direct effect, i.e. absorption and re-emission of longwave radiation, and on the other hand, via in-direct effects on clouds, altering their brightness, lifetime, occurrence and vertical scale.

During RV METEOR cruise 154/1 aerosol optical depth measurements from the Microtops II sun photometers were recorded for the Maritime Aerosol Network (MAN) component of AERONET. MAN data provide an alternative to observations from islands as well as establish validation points for satellite and aerosol transport models. Since 2004, these instruments have been deployed periodically on ships of opportunity and research vessels to monitor aerosol properties over the World Oceans.

The project is documented and the data can be accessed at: https://aeronet.gsfc.nasa.gov/new_web/maritime_aerosol_network.html.

5.3.1 System setup

Naturally measurements must be carried out during daytime, only when there is no cloud obscuring the sun. The instrument is directed towards the sun and measurements are conducted every 20 minutes and consist of 10 scans.

Microtops instruments currently in the network have five channels but they may have one of two configurations: 340, 440, 675, 870, 936nm or 440, 500, 675, 870, and 936nm. In addition, the instrument has built-in temperature and pressure sensors as well as the ability to log accurate time and geographical position using a GPS. The Microtops instruments are calibrated at the NASA Goddard Space Flight Center (GSFC) calibration facility via a transfer calibration procedure between the Microtops and the master Cimel sun photometer at GSFC, which has a calibration traceable to a Langley calibration of a Cimel sun photometer on Mauna Loa, Hawaii. In general, the estimated uncertainty of the aerosol optical depth in each channel does not exceed plus or minus 0.02, which is slightly higher than the uncertainty of AERONET field (not master) instruments.

5.3.2 Preliminary results

Figure 5.24 shows the coarse mode fraction of aerosol optical depth. The further west the less of coarse, Saharan dust aerosol was measured. However, in the Caribbean the property increased again, indicating the proximity to the volcano of Montserrat and its emission of coarse volcanic aerosol.

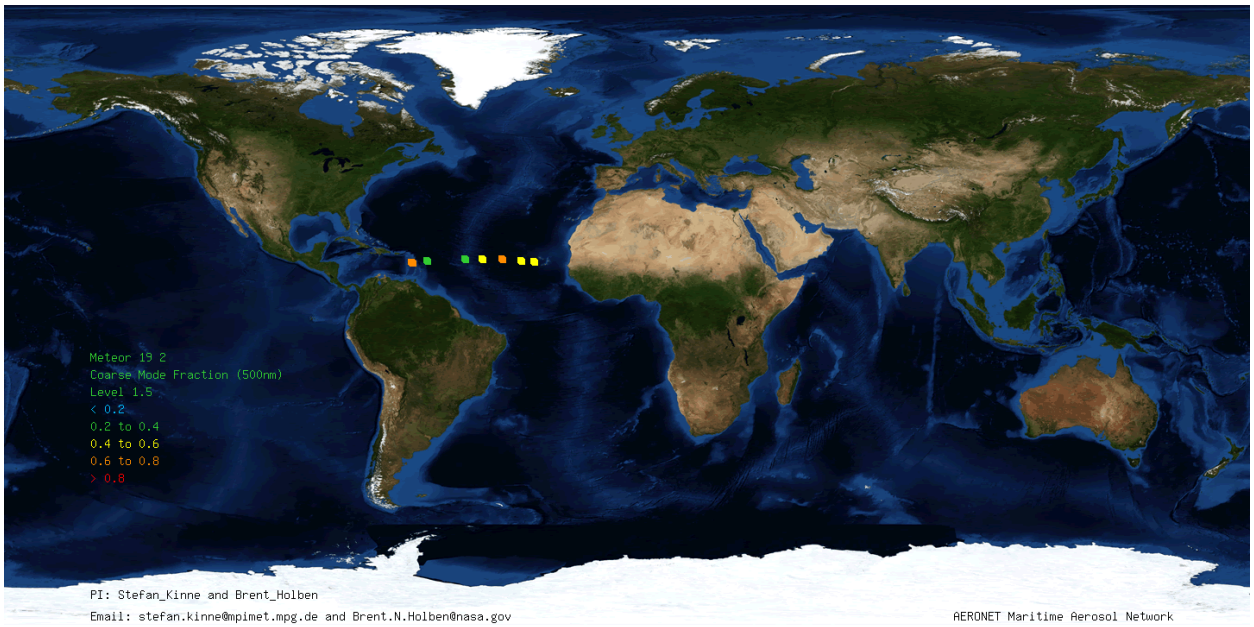

Fig. 5.24: Coarse mode fraction of aerosol optical depth.

6 Ship's Meteorological Station

On the 3rd of April 2019, RV METEOR left at 9 am the port of Mindelo/Cape Verde. During the transit to Guadeloupe, the ship was under the influence of a fresh northeast trade wind. These winds blew between a high over the North Atlantic and the inner tropical convergence zone with about 5 Bft. Short after leaving the coast, an approx. 2 m high swell from north was noticeable.

During the next 7 days of transit, RV METEOR stayed under the influence of the above mentioned high with occasional bigger cloud banks. Close to the end of the transit both wind and swell turned to east with consistent strengths.

On April the 10th, RV METEOR reached the research area southeasterly of Montserrat and was now on the southwesterly rim of the still steady high over the North Atlantic. The now easterly air flow brought partially damp air to the research area with scattered showers.

The wind blew furthermore with approx. 5 Bft, partly 6 and rose only during the night of the 13th to 14th of April for a couple of hours to 7 Bft. The significant wave height was steady with 1.5 to 2 m with an easterly swell.

Fig. 6.1: Southeast coast of Montserrat during the RV METEOR Cruise M154/1 (Photo M. Stelzner).

Around the 12th of April, a new high developed along the northeast coast of America. During the following days the high intensified, travelled southeast and turned into a strong high over the North Atlantic. However, the only change in the weather situation could be seen in the slight decrease of the wind down to 5 Bft, at times even 4 Bft.

At the end of the journey, there was a bit of movement in the weather situation. Between the strong Atlantic high and a new smaller high along the American east coast, a deep trough coming from a low at Newfoundland spread towards south. On the 20th of April, this trough developed into a low which first deepened and then moved southwesterly towards the Lesser Antilles. On the 23rd of April, this low, which was in adequate distance to the research area, slowed down and turned towards northwest. That brought very low pressure differences for the last days of the journey M154/1. The now from northeast coming wind decreased to less than 4 Bft. There was hardly any wind sea and the significant wave height stayed under 1.5 m.

The journey ended on the morning of the 25th of April at the harbor of Point-á-Pitre with very calm and sunny weather.

7 Station List M154/1

7.1 Overall Station List

Station No.	Date	Gear	Time	Latitude	Longitude	Water Depth	Remarks/Recovery
METEOR	2019		[UTC]	[°N]	[°W]	[m]	
M154/1_0_Underway-1	4.4	Deep-sea Multibeam Echosounder	04:01	17°08.020'	028°52.123'	4725	profile start
M154/1_0_Underway-1	4.4	P-70 Parasound	04:01	17°08.020'	028°52.123'	4725	profile start
M154/1_0_Underway-2	4.4	Sound Velocity Profiler	04:01	17°08.020'	028°52.124'	4724	W2, Vorgewicht, in the water
M154/1_0_Underway-2	4.4	Sound Velocity Profiler	04:04	17°08.020'	028°52.123'	4724	SVP, SL = 10m, in the water
M154/1_1-1	4.4	Sound Velocity Profiler	05:27	17°08.021'	028°52.124'	4723	SLmax = 4650m, max depth/on ground
M154/1_1-1	4.4	Sound Velocity Profiler	06:57	17°08.022'	028°52.127'	4725	on deck
M154/1_1-1	9.4	Deep-sea Multibeam Echosounder	18:30	17°00.357'	057°35.313'	5837	Unterbrechung Datenaufzeichnung, Eintritt EEZ Frankreich, profile end
M154/1_1-1	9.4	P-70 Parasound	18:30	17°00.357'	057°35.313'	5837	Unterbrechung Datenaufzeichnung, Eintritt EEZ Frankreich, profile end
M154/1_2-1	10.4	Sound Velocity Profiler	14:57	16°37.001'	062°02.013'	1130	W2, mit Releaser-Test, in the water
M154/1_2-1	10.4	Sound Velocity Profiler	15:19	16°37.001'	062°02.013'	1130	SLmax = 1100m, max depth/on ground
M154/1_2-1	10.4	Sound Velocity Profiler	15:22	16°37.000'	062°02.012'	1128	Hydrophon, in the water
M154/1_2-1	10.4	Sound Velocity Profiler	15:24	16°37.001'	062°02.012'	1129	Hydrophon, on deck
M154/1_2-1	10.4	Sound Velocity Profiler	15:28	16°37.001'	062°02.012'	1128	Hydrophon, in the water
M154/1_2-1	10.4	Sound Velocity Profiler	15:33	16°37.001'	062°02.012'	1129	Hydrophon, on deck
M154/1_2-1	10.4	Sound Velocity Profiler	15:33	16°37.002'	062°02.012'	1130	Hydrophon, in the water
M154/1_2-1	10.4	Sound Velocity Profiler	16:01	16°37.001'	062°02.012'	1131	Hydrophon, on deck
M154/1_2-1	10.4	Sound Velocity Profiler	16:03	16°37.000'	062°02.012'	1131	Hydrophon, in the water
M154/1_2-1	10.4	Sound Velocity Profiler	16:14	16°37.002'	062°02.013'	1131	Hydrophon, on deck
M154/1_2-1	10.4	Sound Velocity Profiler	16:14	16°37.002'	062°02.012'	1131	hoisting
M154/1_2-1	10.4	Sound Velocity Profiler	16:38	16°37.001'	062°02.012'	1131	on deck
M154/1_3-1	10.4	Seismic Ocean Bottom Receiver	19:10	16°39.995'	062°02.949'	1082	OBS 1, OBS deployed
M154/1_4-1	10.4	Seismic Ocean Bottom Receiver	19:37	16°39.347'	062°01.603'	1106	OBS 2, OBS deployed
M154/1_5-1	10.4	Seismic Ocean Bottom Receiver	20:02	16°38.772'	062°00.476'	1109	OBS 3, OBS deployed
M154/1_6-1	10.4	Seismic Ocean Bottom Receiver	20:27	16°38.132'	061°59.429'	1119	OBS 4, OBS deployed
M154/1_7-1	10.4	Seismic Ocean Bottom Receiver	21:16	16°35.492'	061°54.434'	1158	OBS 5, OBS deployed
M154/1_8-1	10.4	Seismic Ocean Bottom Receiver	21:59	16°31.030'	061°57.022'	1178	OBS 6, OBS deployed
M154/1_9-1	10.4	Seismic Ocean Bottom	22:32	16°32.992'	061°58.266'	1160	OBS 7, OBS deployed

			Receiver					
M154/1_10-1		10.4	Seismic Ocean Bottom Receiver	22:58	16°34.749'	061°59.464'	1154	OBS 8, OBS deployed
M154/1_11-1		10.4	Seismic Ocean Bottom Receiver	23:24	16°36.638'	062°00.676'	1137	OBS 9, OBS deployed
M154/1_12-1		10.4	Seismic Ocean Bottom Receiver	23:50	16°38.443'	062°01.895'	1113	OBS 10, OBS deployed
M154/1_13-1		11.4	Seismic Towed Receiver	00:17	16°38.456'	062°01.358'	1114	Airgun in water
M154/1_13-1		11.4	Seismic Towed Receiver	00:27	16°38.395'	062°01.030'	1119	Streamer, information
M154/1_13-1		11.4	Seismic Towed Receiver	03:48	16°44.024'	062°05.681'	885	profile start
M154/1_13-1		11.4	Seismic Towed Receiver	16:14	16°42.272'	062°07.380'	703	profile end
M154/1_13-1		11.4	Seismic Towed Receiver	16:37	16°42.734'	062°07.109'	715	Streamer, on deck
M154/1_13-1		11.4	Seismic Towed Receiver	16:49	16°42.546'	062°06.774'	779	Airgun, on deck
M154/1_0_Underway-3		11.4	Deep-sea Multibeam Echosounder	00:29	16°38.390'	062°00.993'	1120	profile start
M154/1_0_Underway-3		11.4	P-70 Parasound	00:29	16°38.388'	062°00.983'	1119	profile start
M154/1_0_Underway-3		11.4	Seismic Towed Receiver	17:54	16°40.397'	062°03.415'	1072	Stb-Scherbrett im Wasser, information
M154/1_0_Underway-3		11.4	Seismic Towed Receiver	19:38	16°37.888'	062°00.529'	1123	Bb-Scherbrett im Wasser, information
M154/1_0_Underway-3		11.4	Seismic Towed Receiver	20:38	16°36.444'	061°58.872'	1139	Airgun in water
M154/1_0_Underway-3		11.4	Seismic Towed Receiver	21:55	16°35.380'	061°56.326'	1000	profile start
M154/1_0_Underway-4		12.4	Seismic Towed Receiver	01:31	16°38.946'	062°00.983'	1109	Airgun, on deck
M154/1_0_Underway-4		12.4	Seismic Towed Receiver	05:45	16°34.818'	061°53.067'	1026	Airgun in water
M154/1_0_Underway-4		12.4	Seismic Towed Receiver	18:39	16°36.028'	061°57.092'	988	Airgun, on deck
M154/1_0_Underway-4		12.4	Seismic Towed Receiver	20:10	16°36.598'	061°55.580'	1063	Beginn Aussetzen, information
M154/1_0_Underway-4		12.4	Seismic Towed Receiver	20:12	16°36.599'	061°55.550'	1033	Bb-Scherbrett zu Wasser, information
M154/1_0_Underway-4		12.4	Seismic Towed Receiver	20:40	16°36.544'	061°55.014'	1075	Airgun in water
M154/1_14-1		13.4	Seismic Towed Receiver	04:33	16°38.956'	062°02.276'	1108	profile end
M154/1_14-1		13.4	Seismic Towed Receiver	04:57	16°39.295'	062°02.079'	1104	Airgun, on deck
M154/1_14-1		13.4	Seismic Towed Receiver	06:26	16°39.104'	062°00.498'	1107	Bb-Scherbrett, on deck
M154/1_14-1		13.4	Seismic Towed Receiver	06:43	16°39.101'	062°00.255'	1104	Stb-Scherbrett, on deck
M154/1_14-1		13.4	Seismic Towed Receiver	08:41	16°38.829'	061°59.419'	1109	streamer zu Wasser, information
M154/1_14-1		13.4	Seismic Towed Receiver	09:09	16°38.847'	061°58.810'	1066	Airgun in water
M154/1_14-1		13.4	Seismic Towed Receiver	12:19	16°41.646'	062°01.092'	1065	profile start
M154/1_14-1		14.4	Seismic Towed Receiver	14:06	16°36.678'	062°00.414'	1136	Airgun, on deck
M154/1_14-1		14.4	Seismic Towed Receiver	15:48	16°38.641'	061°59.019'	1102	Airgun in water

M154/1_14-1		15.4	Seismic Towed Receiver	15:28	16°43.394'	062°07.374'	645	profile end
M154/1_14-1		15.4	Seismic Towed Receiver	15:49	16°43.988'	062°07.276'	693	Airgun, on deck
M154/1_14-1		15.4	Seismic Towed Receiver	16:08	16°44.166'	062°06.846'	811	Streamer, on deck
M154/1_14-1		15.4	Seismic Towed Receiver	19:37	16°37.469'	062°05.039'	1065	Bb-Scherbrett zu Wasser, information
M154/1_14-1		15.4	Seismic Towed Receiver	19:49	16°37.517'	062°04.873'	1071	Stb-Scherbrett zu Wasser, information
M154/1_15-1		16.4	Seismic Towed Receiver	00:03	16°38.237'	062°00.670'	1116	Streamer zu Wasser, information
M154/1_15-1		16.4	Seismic Towed Receiver	00:30	16°38.509'	062°00.031'	1111	Airgun in water
M154/1_15-1		16.4	Seismic Towed Receiver	00:58	16°38.008'	061°58.772'	977	profile start
M154/1_15-1		16.4	Seismic Towed Receiver	12:56	16°40.243'	062°01.681'	1086	Airgun, on deck
M154/1_15-1		16.4	Seismic Towed Receiver	13:50	16°40.870'	062°00.563'	1085	Airgun in water
M154/1_15-1		17.4	Seismic Towed Receiver	10:00	16°39.524'	062°01.002'	1106	Airgun an Deck, information
M154/1_15-1		17.4	Seismic Towed Receiver	10:27	16°39.232'	062°00.405'	1102	Stb-Scherbrett dichtgeholt, information
M154/1_15-1		17.4	Seismic Towed Receiver	11:39	16°38.696'	061°59.237'	1108	Stb-Scherbrett wieder ausgebracht, information
M154/1_16-1		17.4	Seismic Towed Receiver	13:32	16°37.559'	061°57.469'	652	Airgun in water
M154/1_16-1		17.4	Seismic Towed Receiver	16:25	16°38.951'	062°00.837'	1108	Airgun, on deck
M154/1_16-1		17.4	Seismic Towed Receiver	17:55	16°38.537'	061°58.763'	1015	Airgun in water
M154/1_16-1		18.4	Seismic Towed Receiver	02:54	16°36.616'	061°56.564'	769	profile end
M154/1_16-1		18.4	Seismic Towed Receiver	03:03	16°36.565'	061°56.365'	761	Airgun, on deck
M154/1_16-1		18.4	Seismic Towed Receiver	04:00	16°36.175'	061°55.074'	1131	Streamer, on deck
M154/1_16-1		18.4	Seismic Towed Receiver	05:52	16°35.617'	061°53.545'	1078	Bb-Scherbrett, on deck
M154/1_16-1		18.4	Seismic Towed Receiver	06:06	16°35.530'	061°53.361'	1056	Stb-Scherbrett, on deck
M154/1_16-1		18.4	Seismic Towed Receiver	06:56	16°35.297'	061°52.806'	996	2D, Airgun in water
M154/1_16-1		18.4	Seismic Towed Receiver	07:03	16°35.252'	061°52.704'	988	Streamer zu Wasser, information
M154/1_16-1		18.4	Seismic Towed Receiver	08:14	16°36.969'	061°54.691'	1021	profile start
M154/1_16-1		18.4	Seismic Towed Receiver	20:42	16°35.162'	062°08.729'	900	Streamer an Deck, information
M154/1_16-1		18.4	Seismic Towed Receiver	22:40	16°36.790'	062°02.316'	1132	profile end
M154/1_16-1		18.4	Seismic Towed Receiver	22:49	16°36.796'	062°02.160'	1134	Airgun an Deck, information
M154/1_16-1		18.4	Seismic Towed Receiver	23:08	16°36.863'	062°01.843'	1133	Stb Scherbrett zu Wasser, information
M154/1_16-1		18.4	Seismic Towed Receiver	23:20	16°36.918'	062°01.639'	1126	Bb Scherbrett zu Wasser, information
M154/1_16-1		19.4	Seismic Towed Receiver	00:41	16°37.191'	062°00.403'	1130	Streamer zu Wasser, information
M154/1_16-1		19.4	Seismic Towed Receiver	00:48	16°37.214'	062°00.335'	1129	Airgun in water

M154/1_17-1		19.4	Seismic Towed Receiver	06:00	16°39.640'	062°02.209'	1104	profile start
M154/1_17-1		20.4	Seismic Towed Receiver	18:17	16°38.570'	062°00.323'	1115	Unterbrechung, profile end
M154/1_17-1		20.4	Seismic Towed Receiver	18:38	16°38.923'	062°00.523'	1108	Airgun, on deck
M154/1_17-1		20.4	Seismic Towed Receiver	21:22	16°39.183'	061°58.421'	989	Airgun in water
M154/1_17-1		20.4	Seismic Towed Receiver	22:20	16°38.396'	062°00.092'	1118	Fortsetzung, profile start
M154/1_17-1		21.4	P-70 Parasound	17:13	16°37.518'	061°59.766'	1125	profile end
M154/1_18-1		22.4	Expendable Bathythermograph	19:14	16°36.170'	061°56.581'	851	in the water
M154/1_18-1		23.4	Deep-sea Multibeam Echosounder	18:11	16°39.883'	062°01.034'	1098	Unterbrechung, profile end
M154/1_18-1		23.4	Deep-sea Multibeam Echosounder	22:50	16°37.969'	061°59.780'	1119	Fortsetzung, profile start
M154/1_18-1		23.4	P-70 Parasound	22:50	16°37.966'	061°59.785'	1118	Fortsetzung, profile start
M154/1_18-1		23.4	Seismic Towed Receiver	16:40	16°39.694'	062°02.184'	1102	profile end
M154/1_18-1		23.4	Seismic Towed Receiver	17:02	16°40.249'	062°02.285'	1086	Airgun, on deck
M154/1_18-1		23.4	Seismic Towed Receiver	17:58	16°39.975'	062°01.256'	1090	Streamer, Datenkabel, on deck
M154/1_18-1		23.4	Seismic Towed Receiver	18:23	16°39.801'	062°00.844'	1098	Stb-Scherbrett, on deck
M154/1_18-1		23.4	Seismic Towed Receiver	18:32	16°39.752'	062°00.677'	1098	Bb-Scherbrett, on deck
M154/1_18-1		23.4	Seismic Ocean Bottom Receiver	19:00	16°39.808'	062°01.778'	1098	Hydrophon zu Wasser, information
M154/1_18-1		23.4	Seismic Ocean Bottom Receiver	19:01	16°39.801'	062°01.803'	1098	ausgelöst, information
M154/1_18-1		23.4	Seismic Ocean Bottom Receiver	19:05	16°39.776'	062°01.896'	1098	Hydrophon an Deck, information
M154/1_18-1		23.4	Seismic Ocean Bottom Receiver	19:26	16°40.000'	062°03.428'	1098	Hydrophon zu Wasser, information
M154/1_18-1		23.4	Seismic Ocean Bottom Receiver	19:37	16°39.950'	062°03.382'	1098	Hydrophon an Deck, information
M154/1_19-1		23.4	Seismic Ocean Bottom Receiver	19:47	16°39.849'	062°03.441'	1098	Hydrophon zu Wasser, information
M154/1_20-1		23.4	Seismic Ocean Bottom Receiver	20:01	16°39.717'	062°03.752'	1098	Hydrophon an Deck, information
M154/1_20-1		23.4	Seismic Ocean Bottom Receiver	20:09	16°39.777'	062°03.690'	1098	aufgetaucht, information
M154/1_20-1		23.4	Seismic Ocean Bottom Receiver	20:25	16°39.880'	062°03.226'	1098	on deck
M154/1_20-1		23.4	Seismic Ocean Bottom Receiver	20:28	16°39.846'	062°03.243'	1098	Hydrophon z/W, information
M154/1_20-1		23.4	Seismic Ocean Bottom Receiver	20:29	16°39.838'	062°03.252'	1098	ausgelöst, information
M154/1_20-1		23.4	Seismic Ocean Bottom Receiver	20:34	16°39.787'	062°03.340'	1098	Hydrophon a/D, information
M154/1_20-1		23.4	Seismic Ocean Bottom Receiver	20:57	16°39.594'	062°02.565'	1098	aufgetaucht, information
M154/1_20-1		23.4	Seismic Ocean Bottom Receiver	21:11	16°39.185'	062°02.032'	1098	angepickt, information
M154/1_20-1		23.4	Seismic Ocean Bottom Receiver	21:13	16°39.162'	062°02.036'	1098	on deck
M154/1_21-1		23.4	Seismic Ocean Bottom Receiver	21:13	16°39.161'	062°02.036'	1098	Hydrophon z/W, information
M154/1_21-1		23.4	Seismic Ocean Bottom	21:14	16°39.153'	062°02.042'	1098	ausgelöst, information

			Receiver					
M154/1_21-1		23.4	Seismic Ocean Bottom Receiver	21:17	16°39.137'	062°02.067'	1098	Hydrophon a/D, information
M154/1_21-1		23.4	Seismic Ocean Bottom Receiver	21:30	16°38.968'	062°01.337'	1098	aufgetaucht, information
M154/1_21-1		23.4	Seismic Ocean Bottom Receiver	21:46	16°38.712'	062°00.791'	1098	angepickt, information
M154/1_21-1		23.4	Seismic Ocean Bottom Receiver	21:48	16°38.693'	062°00.783'	1098	on deck
M154/1_22-1		23.4	Seismic Ocean Bottom Receiver	21:48	16°38.690'	062°00.784'	1098	Hydrophon z/W, information
M154/1_22-1		23.4	Seismic Ocean Bottom Receiver	21:50	16°38.680'	062°00.796'	1098	ausgelöst, information
M154/1_22-1		23.4	Seismic Ocean Bottom Receiver	21:54	16°38.656'	062°00.849'	1098	Hydrophon a/D, information
M154/1_22-1		23.4	Seismic Ocean Bottom Receiver	22:11	16°38.262'	061°59.942'	1098	gesichtet, information
M154/1_22-1		23.4	Seismic Ocean Bottom Receiver	22:23	16°38.076'	061°59.693'	1098	angepickt, information
M154/1_22-1		23.4	Seismic Ocean Bottom Receiver	22:26	16°38.051'	061°59.658'	1098	on deck
M154/1_23-1		24.4	Deep-sea Multibeam Echosounder	09:40	16°35.332'	061°54.331'	1158	Unterbrechung, profile end
M154/1_23-1		24.4	Deep-sea Multibeam Echosounder	15:58	16°38.224'	062°02.299'	1125	Fortsetzung, profile start
M154/1_23-1		24.4	P-70 Parasound	09:40	16°35.346'	061°54.337'	1158	Unterbrechung, profile end
M154/1_23-1		24.4	P-70 Parasound	15:57	16°38.224'	062°02.298'	1126	Fortsetzung, profile start
M154/1_23-1		24.4	Seismic Ocean Bottom Receiver	09:53	16°35.387'	061°54.656'	1162	Hydrophon z/W, information
M154/1_23-1		24.4	Seismic Ocean Bottom Receiver	09:55	16°35.352'	061°54.653'	1162	ausgelöst, information
M154/1_24-1		24.4	Seismic Ocean Bottom Receiver	09:58	16°35.315'	061°54.661'	1162	Hydrophon a/D, information
M154/1_24-1		24.4	Seismic Ocean Bottom Receiver	10:12	16°35.383'	061°54.658'	1162	gesichtet, information
M154/1_24-1		24.4	Seismic Ocean Bottom Receiver	10:25	16°35.368'	061°54.701'	1162	angepickt, information
M154/1_24-1		24.4	Seismic Ocean Bottom Receiver	10:27	16°35.361'	061°54.717'	1162	on deck
M154/1_24-1		24.4	Seismic Ocean Bottom Receiver	11:03	16°31.955'	061°56.703'	1162	Hydrophon z/W, information
M154/1_24-1		24.4	Seismic Ocean Bottom Receiver	11:04	16°31.940'	061°56.729'	1162	ausgelöst, information
M154/1_25-1		24.4	Seismic Ocean Bottom Receiver	11:10	16°31.869'	061°56.834'	1162	Hydrophon a/D, information
M154/1_25-1		24.4	Seismic Ocean Bottom Receiver	11:24	16°30.870'	061°57.180'	1162	gesichtet, information
M154/1_25-1		24.4	Seismic Ocean Bottom Receiver	11:31	16°30.898'	061°57.190'	1162	angepickt, information
M154/1_25-1		24.4	Seismic Ocean Bottom Receiver	11:33	16°30.885'	061°57.198'	1162	on deck
M154/1_25-1		24.4	Seismic Ocean Bottom Receiver	11:34	16°30.872'	061°57.210'	1162	Hydrophon z/W, information
M154/1_25-1		24.4	Seismic Ocean Bottom Receiver	11:35	16°30.867'	061°57.215'	1162	ausgelöst, information
M154/1_26-1		24.4	Seismic Ocean Bottom Receiver	11:38	16°30.848'	061°57.230'	1162	Hydrophon a/D, information
M154/1_26-1		24.4	Seismic Ocean Bottom Receiver	11:50	16°31.638'	061°57.744'	1162	gesichtet, information
M154/1_26-1		24.4	Seismic Ocean Bottom Receiver	12:14	16°32.749'	061°58.646'	1162	angepickt, on deck

M154/1_26-1		24.4	Seismic Ocean Bottom Receiver	12:14	16°32.749'	061°58.646'	1162	Hydrophon, in the water
M154/1_26-1		24.4	Seismic Ocean Bottom Receiver	12:15	16°32.747'	061°58.660'	1162	ausgelöst, information
M154/1_27-1		24.4	Seismic Ocean Bottom Receiver	12:32	16°33.793'	061°59.453'	1162	aufgetaucht, information
M154/1_27-1		24.4	Seismic Ocean Bottom Receiver	12:53	16°34.493'	061°59.873'	1162	on deck
M154/1_27-1		24.4	Seismic Ocean Bottom Receiver	12:53	16°34.493'	061°59.873'	1162	Hydrophon, in the water
M154/1_27-1		24.4	Seismic Ocean Bottom Receiver	12:53	16°34.488'	061°59.877'	1162	ausgelöst, information
M154/1_28-1		24.4	Seismic Ocean Bottom Receiver	13:10	16°35.286'	062°00.386'	1162	aufgetaucht, information
M154/1_28-1		24.4	Seismic Ocean Bottom Receiver	13:35	16°36.498'	062°01.189'	1162	on deck
M154/1_28-1		24.4	Seismic Ocean Bottom Receiver	13:35	16°36.498'	062°01.189'	1162	Hydrophon, in the water
M154/1_28-1		24.4	Seismic Ocean Bottom Receiver	13:35	16°36.498'	062°01.197'	1162	ausgelöst, information
M154/1_29-1		24.4	Seismic Ocean Bottom Receiver	13:51	16°37.556'	062°01.840'	1162	aufgetaucht, information
M154/1_29-1		24.4	Seismic Ocean Bottom Receiver	14:10	16°38.278'	062°02.287'	1121	on deck
M154/1_29-1		24.4	Sound Velocity Profiler	14:36	16°38.225'	062°02.297'	1121	in the water
M154/1_29-1		24.4	Sound Velocity Profiler	15:00	16°38.225'	062°02.298'	1121	SLmax = 1100m, max depth/on ground
M154/1_30-1		24.4	Sound Velocity Profiler	15:33	16°38.224'	062°02.298'	1122	on deck
M154/1_30-1		25.4	Deep-sea Multibeam Echosounder	02:28	16°33.728'	062°05.513'	954	profile end
M154/1_30-1		25.4	P-70 Parasound	02:27	16°33.728'	062°05.532'	952	profile end

7.2 Ocean bottom seismometer Station List

	Deployment				Recovery				
OBS No.	Latitude	Longitude	Depth/m	Time/UTC	Latitude	Longitude	Date/UTC	Time released/UTC	Time recovered/UTC
OBS01	16°39.334 N	62°02.949 W	1084	10.04.2019 19:10	16°39.880 N	62°03.226 W	23.04.2019	19:01	20:24
OBS02	16°39.346 N	62°01.603 W	1106	10.04.2019 19:38	16°39.178 N	62°02.031 W	23.04.2019	20:29	21:11
OBS03	16°38.773 N	62°00.479 W	1109	10.04.2019 20:03	16°38.688 N	62°00.789 W	23.04.2019	21:14	21:48
OBS04	16°38.134 N	61°59.437 W	1120	10.04.2019 20:28	16°38.066 N	61°59.669 W	23.04.2019	21:50	22:24
OBS05	16°35.489 N	61°54.435 W	1157	10.04.2019 21:16	16°34.365 N	61°54.710 W	24.04.2019	09:55	10:12
OBS06	16°31.033 N	61°57.019 W	1180	10.04.2019 22:00	16°30.875 N	61°57.208 W	24.04.2019	11:04	11:33
OBS07	16°32.993 N	61°58.267 W	1162	10.04.2019 22:33	16°32.749 N	61°58.648 W	24.04.2019	11:34	11:52
OBS08	16°34.747 N	61°59.464 W	1154	10.04.2019 22:58	16°34.535 N	61°59.860 W	24.04.2019	12:15	12:48
OBS09	16°36.635 N	62°00.676 W	1137	10.04.2019 23:23	16°36.496 N	62°01.147 W	24.04.2019	12:53	13:29
OBS10	16°38.443 N	62°01.896 W	1114	10.04.2019 23:50	16°38.301 N	62°02.271 W	24.04.2019	13:35	14:07

7.3 2D seismic profiles Station List

	Start		End	
Name	Latitude	Longitude	Latitude	Longitude
P5000	16° 37.9180' N	61° 57.3257' W	16° 42.0573' N	62° 1.30478' W
P5001	16° 41.8076' N	62° 0.77070' W	16° 38.8850' N	62° 5.68904' W
P5002	16° 38.9834' N	62° 5.88897' W	16° 41.1055' N	62° 5.26214' W
P5003A	16° 41.1143' N	62° 5.21441' W	16° 38.8694' N	62° 3.47570' W
P5003B	16° 38.8671' N	62° 3.47621' W	16° 29.1500' N	61° 56.9621' W
P5004	16° 29.1551' N	61° 57.5369' W	16° 30.4167' N	61° 55.3610' W
P5005	16° 30.0622' N	61° 55.6739' W	16° 42.7108' N	62° 3.65386' W
P5006	16° 42.6277' N	62° 3.17538' W	16° 41.0624' N	62° 4.89509' W
P5007	16° 41.4903' N	62° 5.22113' W	16° 34.0806' N	61° 51.4394' W
P5008	16° 33.9111' N	61° 51.4493' W	16° 28.8710' N	62° 1.36676' W
P5009	16° 28.8884' N	62° 1.39583' W	16° 29.9479' N	62° 2.01425' W
P5010	16° 30.3974' N	62° 2.19692' W	16° 36.6902' N	61° 52.2391' W
P5011	16° 36.0812' N	61° 52.3361' W	16° 38.6965' N	61° 54.3272' W
P5012	16° 38.2631' N	61° 53.8160' W	16° 32.9841' N	62° 2.64773' W
P5013	16° 33.2583' N	62° 2.77465' W	16° 35.2760' N	62° 1.38970' W
P5014	16° 38.6912' N	61° 58.1899' W	16° 36.9161' N	62° 5.48561' W
P5015	16° 36.9575' N	62° 5.60313' W	16° 48.7112' N	62° 7.85189' W
P5016	16° 48.7974' N	62° 7.61525' W	16° 27.3789' N	61° 54.5424' W
P5017	16° 27.3766' N	61° 55.1432' W	16° 40.1191' N	61° 55.5993' W
P5018	16° 39.8292' N	61° 55.1846' W	16° 33.8959' N	62° 5.37614' W
P5019	16° 35.8610' N	62° 6.48453' W	16° 39.4751' N	61° 59.0253' W
P6000	16° 34.6811' N	61° 52.9378' W	16° 36.8794' N	61° 54.5884' W
P6001	16° 36.8880' N	61° 54.5980' W	16° 41.0286' N	62° 2.22531' W
P6002	16° 41.0815' N	62° 2.25225' W	16° 47.2381' N	62° 2.22489' W
P6003	16° 47.1057' N	62° 1.66794' W	16° 38.0529' N	62° 8.47399' W
P6004	16° 38.0379' N	62° 8.50913' W	16° 37.7936' N	62° 14.7270' W
P6005	16° 36.9655' N	62° 14.7638' W	16° 37.1151' N	62° 8.33891' W
P6006	16° 36.1249' N	62° 8.30399' W	16° 36.0288' N	62° 14.3001' W
P6007	16° 35.1205' N	62° 14.2804' W	16° 35.1596' N	62° 9.00761' W

8 Data and Sample Storage and Availability

A short cruise report was submitted to Leitstelle Deutsche Forschungsschiffe directly after the cruise. The GEOMAR data management team provides data storage for marine science projects in the Ocean Science Information System (OSIS). All metadata are immediately available publicly via the following link pointing at the GEOMAR data management portal (https://portal.geomar.de/metadata/leg/show/348688). Responsible persons for the different datasets are listed in Table 8.1

After three years the data management team assists to publish these data sets in the World Data Centre PANGAEA (Data Publisher for Earth & Environmental Science), i.e. by May, 2022.

The aerosol measurement data can be accessed on the following website: https://aeronet.gsfc.nasa.gov/new_web/maritime_aerosol_network.html.

Data	Responsible Person	Affiliation	Email
Seismic data	Berndt, Christian	GEOMAR	cberndt@geomar.de
Parasound data	Berndt, Christian	GEOMAR	cberndt@geomar.de
Multibeam data	Berndt, Christian	GEOMAR	cberndt@geomar.de
OBS data	Berndt, Christian	GEOMAR	cberndt@geomar.de
Aerosols	Müller, Sebastian	MPI	sebastian.mueller@mpimet.mpg.de

Tab. 8.1: Overview of responsible persons for the different data sets.

9 Acknowledgements

We thank captain Rainer Hammacher and his crew for their relentless support during the voyage. Funding for M154/1 was provided through the German Science Foundation (Project Sekt) and the Helmholtz Association through the core strategic program OCEANS.

10 References

Boudon, G., Le Friant, A., Komorowski, J.-C., Deplus, C. and Semet, M.P., 2007. Volcano flank instability in the Lesser Antilles Arc: diversity of scale, processes, and temporal recurrence. Journal of Geophysical Research, 112.

Crandell, D.R., 1989. Gigantic debris avalanche of pleistocene Age from ancestral Mount Shasta Volcano, California, and debris-avalanche hazard zonation. U.S. Geological Survey Bulletin 1861.

Crutchley, G. J., Karstens, J., Berndt, C., Talling, P. J., Watt, S. F. L., Vardy, M. E., Hühnerbach, V., Urlaub, M., Sarkar, S., Klaeschen, D., Paulatto, M., LeFriant, A., Lebas, E. und Maeno, F. (2013) Insights into the emplacement dynamics of volcanic landslides from high-resolution 3D seismic data acquired offshore Montserrat, Lesser Antilles Marine Geology, 335. 1-15. DOI 10.1016/j.margeo.2012.10.004.

Deplus, C. et al., 2001. Submarine evidence for large-scale debris avalanches in the Lesser Antilles Arc. Earth and Planetary Science Letters, 192: 145-157.

Frey-Martínez, J., Cartwright, J. and James, D., 2006. Frontally confined versus frontally emergent submarine landslides: A 3D seismic characterisation. Marine and Petroleum Geology, 23(5): 585-604.

Labazuy, P., 1996. Recurrent landslides events on the submarine flank of Piton de la Fournaise volcano (Reunion Island). Geological Society, London, Special Publications, 110(1): 295-306.

Lebas, E., Le Friant, A., Boudon, G., Watt, S., Talling, S., Feuillet, N., Deplus, C., Berndt, C.,

and Vardy, M.: "Multiple widespread landslides during the long-term evolution of a volcanic island: insights from high-resolution seismic data, Montserrat, Lesser Antilles", Geochemistry, Geophysics, Geosystems, 12, 5, Q05006, doi:10.1029/2010GC003451, 2011.

Le Friant, A. et al., 2004. Geomorphological evolution of Montserrat (West Indies): importance of flank collapse and erosional processes. J. Geol. Soc. (London, U.K.), 161(1): 147-160.

Lebas, E., Le Friant, A., Boudon, G., Watt, S. F. L., Talling, P. J., Feuillet, N. & Vardy, M. E. (2011). Multiple widespread landslides during the long-term evolution of a volcanic island: Insights from high-resolution seismic data, Montserrat, Lesser Antilles. Geochemistry, Geophysics, Geosystems, 12(5).

Løvholt, F., Harbitza, C.,B. and Haugenb, K.,B. 2005. A parametric study of tsunamis generated by submarine slides in the Ormen Lange/Storegga area off western Norway. An Integrated Study for Safe Field Development in the Storegga Submarine Area Ormen Lange, 219-231

Masson, D.G., Le Bas, T.P., Grevemeyer, I. and Weinrebe, W., 2008. Flank collapse and large-scale landsliding in the Cape Verde Islands, off West Africa. Geochem. Geophys. Geosyst., 9(7): Q07015.

Masson, D.G. et al., 2002. Slope failures on the flanks of the western Canary Islands. Earth Science Reviews, 57: 1-35.

McMurtry, G.M. et al., 2004. Megatsunami deposits on Kohala volcano, Hawaii, from flank collapse of Mauna Loa. Geology, 32(9): 741-744.

Moore, J.G. et al., 1989. Prodigious submarine landslides on the Hawaiian Ridge. Journal of Geophysical Research, 94(B12): 17,465-17,485.

Moore, J.G., Bryan, W.B., Beeson, M.H. and Normark, W.R., 1995. Giant blocks in the South Kona landslide, Hawaii. Geology, 23(2): 125-128.

Moore, J.G. and Normark, W.R., 1994. Giant Hawaiian Landslides. Annual Review of Earth and Planetary Sciences, 22: 119-144.

Krastel, S. and Schmincke, H.-U., 2002. Crustal structure of northern Gran Canaria, Canary Islands, deduced from active seismic tomography. Journal of Volcanology and Geothermal Research, 115(1-2): 153-177.

Krastel, S. et al., 2001. Submarine landslides around the Canary Islands. Journal of Geophysical Research, 106(B3): 3977-3997.

Urgeles, R., Masson, D.G., Canals, M., Watts, A.B. and Le Bas, T.P., 1999. Recurrent large-scale landsliding on the west flank of La Palma, Canary Islands. Journal of Geophysical Research, 104(B11): 25,331-25,348.

Watts, A.B. and Masson, D.G., 1995. A giant landslide on the north flank of Tenerife, Canary Islands. Journal of Geophysical Research, 100(B12): 24,487-24,498.

Watt, S.F.L. et al. Combinations of volcanic-flank and seafloor-sediment failure offshore Montserrat, and their implications for tsunami generation. Earth and Planetary Science Letters, 319-320, 228-240, doi: 10.1016/j.epsl.2011.11.032, 2012a

Watt, S.F.L., Talling, P.J., Vardy, M.E., Masson, D.G., Henstock, T.J., Hühnerbach, V., Minshull, T.A., Urlaub, M., Lebas, E., Le Friant, A., Berndt, C., Crutchley, G.J., and Karstens, J.: "Widespread and progressive seafloor-sediment failure following volcanic debris avalanche emplacement: Landslide dynamics and timing offshore Monserrat, Lesser Antilles", Marine Geology, 323–325, 69–94, 2012b.

Watt, S.F.L., Talling, P.J., Vardy, M.E., Heller, V., Hühnerbach, V., Urlaub, M., Sarkar, S., Masson, D.G., Henstock, T.J., Minshull, T.A., Paulatto, M., Le Friant, A., Lebas, E., Berndt, C., Crutchley, G.J., Karstens, J., Stinton, A.J., and Maeno, F.: "Combinations of volcanic-flank

and seafloor-sediment failure offshore Montserrat, and their implications for tsunami generation", Earth and Planetary Science Letters, 319-320, 228-240, doi: 10.1016/j.epsl.2011.11.032, 2012.

Watt, S.F.L., Karstens, J., Micallef, A., Berndt, C., Urlaub, M., Ray, M., Desai, A., Sammartini, M., Klaucke, I., Böttner, C., Day, S., Downes, H., Kühn, M. and Elger, E., 2019. From catastrophic collapse to multi-phase deposition: Flow transformation, seafloor interaction and triggered eruption following a volcanic-island landslide. Earth and Planetary Science Letters, Volume 517, 135-147. https://doi.org/10.1016/j.epsl.2019.04.024.

Williams, M., Wilkinson, I.P., Tappin, D.R., McMurty, G. and Fryer, G.J., 2006. The Hawaiian megatsunami of 110¬±10 ka: the use of microfossils in detection. Journal of Micropalaeontology, 25(1): 55-56.

Wolfe, C.J., McNutt, M.K. and Detrick, R.S., 1994. The Marquesas archipelagic apron: Seismic stratigraphy and implications for volcano growth, mass wasting, and crustal underplating. Journal of Geophysical Research, 99(B7): 13,591-13,608.

Wynn, R.B. and Masson, D.G., 2003. Canary islands landslides and tsunami generation: Can we suse turbidite deposits to interpret landslide processes? In: J. Locat and J. Mienert (Editors), Submarine mass movements and their consequences. Kluwer Academic Publishers, 325-332

Hunt, J.E., Wynn, R.B., Masson, D.G., Talling, P.J. and Teagle, D.A.H., 2011. Sedimentological and geochemical evidence for multistage failure of volcanic island landslides: A case study from Icod landslide on north Tenerife, Canary Islands. Geochemistry, Geophysics, Geosystems, 12(12), n/a–n/a. http://doi.org/10.1029/2011GC003740

Karstens, J., Crutchley, G. J., Berndt, C. , Talling, B. J., Watt, S. F. L., Hühnerbach, V., Le Friant, A., Lebas, E. und Trofimovs, J., 2013. Emplacement of pyroclastic deposits offshore Montserrat from 3D seismic data. Journal of Volcanology and Geothermal Research, 257 . pp. 1-11. DOI 10.1016/j.jvolgeores.2013.03.004.

11 Abbreviations

P-Cable	High-resolution 3D seismic system
OBS	Ocean bottom seismometer
MeBo	Meeresboden Bohrgerät (MARUM)
EEZ	Exclusive Economic Zone